Fortpflanzung langsamer Wellen längs eines isotropen, inhomogenen, zylindrischen Plasmas

Slow Wave Transmission Modes of an Isotropic Inhomogeneous Cylindrical Hot Plasma

Benedict B. O'Brien Jr.

IPP 3/33 November 1965

INSTITUT FÜR PLASMAPHYSIK

GARCHING BEI MÜNCHEN

INSTITUT FÜR PLASMAPHYSIK

GARCHING BEI MÜNCHEN

Fortpflanzung langsamer Wellen längs eines isotropen, inhomogenen, zylindrischen Plasmas

Slow Wave Transmission Modes of an Isotropic Inhomogeneous Cylindrical Hot Plasma

Benedict B. O'Brien Jr.

IPP 3/33 November 1965

Die nachstehende Arbeit wurde im Rahmen des Vertrages zwischen dem Institut für Plasmaphysik GmbH und der Europäischen Atomgemeinschaft über die Zusammenarbeit auf dem Gebiete der Plasmaphysik durchgeführt.

IPP 3/33 B. O'Brien

Slow Wave Transmission Modes of an Isotropic Inhomogeneous Cylindrical Hot Plasma

November, 1965 (in Englisch)

Abstract

The dispersion relations for coupled electromagnetic waves and longitudinal waves propagating along a plasma column are derived and experimentally measured. The "hot" plasma is described by the equations of the two fluid model which include a gradient pressure term. A quasi-static approximation, $E = -\text{grad}\,\phi$, is used in place of the complete electromagnetic equations. The ω-β curves (β is the propagation constant along the column) have been calculated for modes which have none and one azimuthal variation. The measurements, performed on the positive column of a mercury vapor discharge, show the presence of many bands of propagation corresponding to many nodes in the radial direction. The theoretical and experimental results are in agreement.

Acknowledgements

The author wishes to thank Professor Doctor W. Rollwagen of the Ludwig-Maximilians-University for his support of this work. The author was privileged to carry out this investigation in the Experimental Group of the Max-Planck-Institute for Physics and Astrophysics under the direction of Doctor G. von Gierke. The writer has the pleasure of acknowledging the great number of most valuable discussions with and suggestions made by Professor Doctor R.W. Gould of the California Institute of Technology. Doctor D. Pfirsch of the M.P.I. is gratefully thanked for his assistance in clarifying many aspects of the theoretical consideration. The author's closest collegue, Doctor M. Tutter of the Institute for Plasma Physics, is warmly thanked for his untireing help on and guidence in all parts of this work. For the preparation of technical drawings, aid in experimental work, and excellent managing of all the computer programing the author is indebted to Miss E. Bock.

Table of Contents

Introduction

The phenomena of wave propagation along a plasma column is closely related to the dipole resonances of such a plasma. These resonances which may be refered to the works of Tonks[1] and Romell[2] have often been named Tonks-Dattner resonances because of the extensive experimental investigation by Dattner[3]. The explanation of these resonances has been the subject of many papers. The most complete quantitative analysis is given by Parker, Nickel, and Gould[4]. In this work and in papers by Vandenplas and Gould[5], Vandenplas and Messiaen[6], and Crawford[7] are quite complete lists of relevant papers. As these resonances are not the main subject of this paper the question of literature will not be further discussed here. The results published by Parker, Nickel, and Gould[4] (PNG) will, however, be used to introduce a discussion of the physical mechanism of the propagation phenomena.

An infinite isotropic homogeneous plasma can support propagating transverse electromagnetic waves and propagating longitudinal "plasma waves" if ω, the signal frequency, is larger than ω_p, the plasma frequency. ω_p^2 is equal to $\frac{ne^2}{\varepsilon_0 m_e}$ [8]; n is the electron density, e and m_e the electron charge and mass respectively. In the definition of ω_p the ion mass is considered very large compared with the electron mass. In such an infinite isotropic homogeneous plasma, these two propagating waves are independent of one another.

The electromagnetic wave propagation can be characterized by the introduction of an index of refraction,[9]

$$n_\perp^2 = \left(1 - \frac{\omega_p^2}{\omega^2}\right)\left(1 + \frac{\omega_p^2}{\omega^2}\frac{KT_e}{m_e c^2}\right)^{-1}. \qquad (1)$$

The movement of the ions compared to the electrons is neglected and a thermal electron gas of temperature T_e is

assumed. The second term in the latter parenthesises is of the order of $10^{-5} \frac{\omega_p^2}{\omega^2}$ for the plasmas described in this paper. This term which does not include relativistic corrections is none the less of the order of such corrections. K is the Boltzmann constant and c the velocity of light in vacuum. Since ω_p^2 is the order of magnitude of ω^2 for phenomena considered here, one may neglect the temperature correction term and one has that the index of refraction is order of magnitude of one or less which denotes wavelengths corresponding to or exceeding those in vacuum.

One may also characterize the longitudinal wave propagation by an index of refraction,[9)10)11)]

$$n_{\parallel}^2 = \left(1 - \frac{\omega_p^2}{\omega^2}\right)\left(\frac{3KT_e}{m_e c^2}\right)^{-1} . \qquad (2)$$

The wavelengths involved here are then about 1/300 that of those for the transverse wave.

The "Tonks-Dattner" resonances are the resonances a plasma column demonstrates when a dipole electric field is applied. The vacuum wavelength of the applied signal is large compared to the radius of the column and all variation in the axial direction in neglected. The analysis of this spectrum given by PNG[4)] allows for the existence of both wave types discussed above, and for coupling between them. The wave types here are not independent due to inhomogeneities in the assumed electron density profile and of course the plasma boundary. The results of this analysis which was carried out using a computer show standing waves of the pertubed electron density in the radial direction. The wavelength of the standing wave corresponds quite closely to that calculated from the homogeneous theory (2) using that value of ω_p^2 (which is here a function of radius) which is present at the radial point in question. It is then reasonable to think of these resonances as being caused by waves which propagate in a radial direction being reflected by the glass plasma boundary and, if the plasma is

dense enough, by an overdense region in the middle of the tube. The resonably sharp resonance characteristic of this spectrum comes to be because, for constant ω, only certain plasma densities afford the proper propagation for fulfillment of the boundary conditions.

One may now consider the case where these waves do not travel exclusively in a radial direction but have a component of propagation in the axial direction. An obvious analogue is that of a waveguide in which the waves travel transverse to the guide at cutoff, and travel with a non zero (group) velocity in the axial direction during propagation. The "T-D" resonances represent then, in this picture, the cutoff conditions of modes of propagation. Crawford[7] has also noted that these resonances are special cases of propagation. Just as in the case of waveguide propagation where there are many modes which differ from another only in the number of nodes in the radial direction there are many bands of propagation which also differ from another in a similar way.

These resonances have led to a discussion of bands of propagation which have one azimuthal variation (dipole mode), however, a mode with no azimuthal variation is geometrically simpler. Indeed, the initial experimental investigations were made on this latter mode. The dipole mode will be referred to as $n = 1$ and the rotationally symmetric mode as $n = 0$.

Experiments

Discharge Apparatus:

The experiments reported in this paper were performed on the positive column of a low pressure mercury vapor discharge, Figure 1. The discharge tube is made of Schott 8243 glass. The dimensions are:

Length overall:	84 cm
Distance between probes B and K:	48 cm
Diameter outside:	1.87 cm
Diameter inside:	1.57 cm

The entire discharge tube is housed in a large, 130 x 100 x 30 cm, box which is maintained at a constant temperature of 55°C whereas the temperature of the water bath surrounding the mercury, T_{Hg}, was varied between 15 and 50°C.

Following an initial bake out at 400 °C and many hours of operation it was found that further pumping was unnecessary. The ionization manometer afforded a continuous check on the total pressure in the tube.

The cathode, of the type used in the Valvo PL 5684 thyratron, was heated from a direct current source. The maximum emission of 2 amperes, as recommended by the manufactor, was not exceeded. The cathode is quite robust and in other experiments has shown good tolerance to repeated exposure to the atmosphere (when cold).

A small coil producing a maximum axial field of 30 Gauss, not shown in the figure, was placed around the anode. It was found that at currents of the order of tens of milliamperes and larger that this small concentrated field very materially reduced the small instabilities in anode voltage and current. The instabilities could often be associated with the presence of discharge behind the anode. This "quieting" of the discharge was of great help in the experimental work. At distances of about 15 cm from the anode no direct influence of the field could be detected.

Probes A,B, and K, made of tungston wire 0,5 mm diameter, were inserted to the middle of the tube, however, only the last 2 mm were not insulated with glass.

Measurements

Electron Temperature T_e:

Using probes A and K (no magnetic field) Langmuir[12] probe measurements were made to determine the electron temperature, T_e. For sufficiently large discharge currents (100, 200 and 400 ma) the value of T_e for any given neutral gas pressure, varied generally by only a few percent. Its average value is shown in Figure 2. The dependance of T_e on the discharge current is also shown in Figure 2 for one value of neutral gas pressure (corresponding to 26 °C mercury water bath temperature). Good agreement with a Boltzmann-Maxwell distribution was observed.

Average Electron Density, $\bar{n}_e$, or $\overline{\omega_p^2}$:

The shift in the resonance frequency of a microwave cavity was used to determine the electron density $\bar{n}_e$, averaged over the cross section of the plasma.

$$\overline{\omega_p^2} = \frac{\bar{n}_e e^2}{\epsilon_o m_e} \qquad (3)$$

Measurements were made in transmission through a cylindrical cavity, radius 10.7 cm, length 15 cm, excited in the TM_{o1o} mode and evaluated according to Agdur and Enander[13].

Propagation Measurements; Dipole (n = 1) and Rotationally Symmetric (n = 0) Modes:

The couplers used to launch and detect waves propagating in the n = 0 and 1 modes are shown in Figure 3. In normal operation a pair of identical couplers is used.

The couplers for the n = 0 mode have rotational symmetry except for the connection, at one point, to the generator or detector. The coupler shown in Figure 3a was the first one to be used. It closely resembles the reentrant cavaties often

used for tunable klystrons. With the capacitive loading of the gap it can be tuned from 700 to 2000 Mcps in the "1/4 wavelength mode" and from 1900 to over 4000 Mcps in the "3/4 wavelength mode". The gap width in the device of Figure 3a is 0.5 mm and in the device of Figure 3b 0.5 mm each side of the thin ring. The latter is quite useful at lower frequencies. All the couplers shown in Figure 3 fit closely on the discharge tube and many be moved axially as well as azimuthly.

The generators used to cover the frequency range of measurements, 50 to 4000 Mcps, have a maximum output of about 0.2 watt.

Two basic types of receivers were used in these measurements, first a normal superheterodyne receiver with a sensitivity of about 10^{-13} watt, and second a phase coherent receiver with a sensitivity of about 10^{-11} watt. The phase coherent receiver, developed by the author, was reported in Stockholm in March 1963[14] and is most similar to a receiver reported by Cohn and Weinhouse[15]. Block diagrams of these receivers are shown in Figure 4.

A typical measurement of the n = 0 mode made using a superheterodyne receiver and constant transmitter frequency is shown in Figure 5a. Note that the ordinate is logarithmic. The transmission band which exists at $\omega^2/\overline{\omega_p^2}$ smaller than 0.21 persists as the discharge current, that is, the value of $\overline{\omega_p^2}$, is increased. The discrete bands occuring at higher values of $\omega^2/\overline{\omega_p^2}$ are those which have one or more nodes in the radial standing wave. As observed, the amplitude of the received signal is about 10 times greater in a transmission band than at values of $\omega^2/\overline{\omega_p^2}$ immediately above and below the band. In Figure 5b an ω-β diagram is shown which was measured under the same conditions as 5a. β is equal to $2\pi/\lambda_z$ where λ_z is the wavelength in the axial direction and r_w is radius of the plasma column (0.79 cm). In 5b a phase coherent receiver was used and, at many different values of $\overline{\omega_p^2}$, one of the couplers was moved and the change in phase of the received signal was noted as a function of separation bet-

ween the couplers. Measurements were made propagating in the direction of anode to cathode and vice versa, in order to show the effects of the electron drift velocity. This dispersion diagram shows a similarity to that for a wave guide which was implied in the analogy mentioned in the introduction. The termination of the transmission in each band, at one end, $\beta \rightarrow 0$, is due clearly to cutoff. The observed termination for large β is thought to be caused by Landau damping and poor coupling to the short wave lengths. It will be noted that the word mode is used to denote the azimuthal variation (e.g. n = 0, n = 1 mode) and band to denote a region of transmission of a particular mode.

The zero order stationary radial electron density distribution function decreases monotonly from the middle of the tube, and the fact that ω^2 is often smaller than the $\overline{\omega_p^2}$ means that wave propagation takes place only in a region of the tube near the glass boundary. In this region the value of ω_p^2 is smaller than $\overline{\omega^2}$. The effect of reducing the discharge current is to reduce $\overline{\omega_p^2}$ and the value of ω_p^2 at all points in the tube.

The result of reducing ω_p^2 is to raise the value of the index of refraction or reduce the phase velocity at all points, (where propagation can take place), which has the effect of decreasing the wavelength of the wave traveling in the tube. The reference to "the wave traveling in the tube" is made in analogy to the model of traveling interfering waves often used to explain waveguide propagation[16]. A decrease of wavelength for the traveling waves results then in a decrease in λ_z.

It is obvious that the form of the zero order radial electron distribution function plays an important role in this wave phenomena. Parker[17] has calculated this distribution function for a collisionless plasma and found that one parameter, $r_w^2/\overline{\lambda_d^2}$, is sufficient to characterize its shape. $\overline{\lambda_d^2}$ is the average of the square Debye length defined by equation (4).

$$\lambda_d^2 \equiv \frac{\frac{K T_e}{m_e}}{\omega_p^2} \qquad (4)$$

A further step in the investigation is to look into the dependence of these modes on the r_w^2/λ_d^2 parameter. In order to obtain a simpler picture, a plot of r_w^2/λ_d^2 vs $(\omega^2/\omega_p^2)_{co}$ (the value of ω^2/ω_p^2 corresponding to $\beta r_w = 0$ or C.ut O.ff) is made. This plot is shown in Figure 6, the heavy line along the ordinate denotes the cutoff of first n = 0 band. The $(\omega^2/\omega_p^2)_{co}$ values have been deduced from transmission (between two n = 0 couplers) measurements. It is not expected that direct observation of the cutoff points is possible - see discussion in Theory, Case A.

One may perform similar experiments with the n = 1 mode using appropriate couplers. Figure 7a shows the amplitude of the transmitted signal using a superheterodyne receiver. It was made under conditions similar to those of Figure 5a. Checks of the "dipole characteristics" of the transmission such as orienting the exciter and detector couplers perpendicular to one another disclose that the signal received at values of ω^2/ω_p^2 less than 0.13 is not dipole in nature. Further experiments which will be discussed later show this spurious signal to be effected by coupling to the n = 0 mode. Figure 7b shows the ω-βdiagram measured with a phase coherent receiver corresponding to 7a, here the "n = 0 spurious transmission" has been excluded. The letter "B" denotes observed backward waves - the change in phase of the received signal as the distance between the couplers is increased is opposite in sense to that which is obtained when a line stretcher, in place of the couplers, is lengthened. Except for the region of backward wave propagation and the absence of a mode which extends to $\omega^2/\omega_p^2 \rightarrow 0$ the n = 1 and n = 0 ω - β diagrams are similar. A corresponding plot of r_w^2/λ_d^2 v s $(\omega^2/\omega_p^2)_{co}$ for the n = 1 mode is included in Figure 6. Unfortunately interference with the n = 0 mode precluded measurement of the higher bands of propagation in Figure 7b. Reference to Figure 18, however, shows the similarity to the n = 0 mode indicated here. The plot of cutoff points of the dipole bands of propagation

is, of course, nothing more than a plot of the Tonks-Dattner[1)2)3)4)] resonances.

Measurement of the higher bands of propagation for both the n = 0 and n = 1 modes is considerably more difficult than for the lower bands. This is caused primarily by two factors, first, excitation of and consequently interference with signals of the unwanted azimuthal dependence (n = 0 or 1) and second, the considerably weaker signals received when measuring the higher modes . As is clearly shown in Figure 6 the spacing, in $\omega^2/\overline{\omega_p^2}$, between the cutoff points for the n = 0 and n = 1 higher order bands is quite small. It is then possible that when attempting to observe propagation of a particular band by choosing a value of $\omega^2/\overline{\omega_p^2}$ larger than that for cutoff one might simultaneously excite the unwanted mode. The attenuation of the propagated signal in decibels per cm, along the column is much lower in the region of cutoff than in the region of large β . Should then the value of $\omega^2/\overline{\omega_p^2}$ being used correspond approximately to that of cutoff for the unwanted mode, the interference with the desired signal can be very strong.

Care was taken in the construction of the couplers to reduce extraneous coupling as well as in selection of the glass discharge tube. Small eccentricities in standard glass tubing produce appreciable asymmetry in the coupling to these modes.

On some occasions non-linear effects were observed with r.f. powers comparable to the power dissipated per centimeter in the positive column.

Other Observations:

Some interesting experiments which involve the n = 0 and n = 1 mode as well as the cutoff dipole resonances will now be described. A common method of observing the dipole resonances is sketched in Figure 8. The microwave energy transmitted through the waveguide is recorded as a function of discharge current - or $\overline{\omega_p^2}$. The large distinct transmission minima are the dipole resonance points as shown in Figure 9. Superimposed on this spec-

trum is a second absorption spectrum denoted with the letters α,β, and γ . The magnetic field of the earth, B_E , is perpendicular to the axis of the discharge tube. If the waveguide is oriented so that the electric field of the microwave signal, E_{hf}, is parallel the magnetic field of the earth the minima α,β, and γ disappear. If now one coupler for the rotationally symmetric mode is also mounted on the tube and connected to a superheterodyne receiver tuned to the frequency of the signal in the waveguide, the receiver yields signals as shown in the lower curves of Figure 9. The values of ω^2/ω_p^2 for which α,β, and γ occur, agree with those for the n = 0 modes of propagation. The minimum δ is thought to be the first quadrupole resonance, although no experimental check of this has been made. A discussion of this mode and its excitation is given by Messiaen and Vandenplas[18)19)20)] and by PNG[4)].

A phenomenon similar to that just described is present when transmission between two dipole couplers is observed in the presence of the earth's magnetic field. If the axis of the dipole field of at least one of the dipole couplers is parallel the earth's magnetic field there is transmission only via the n = 1 mode. If, however, both dipole couplers form angles other than zero with B_E, there is transmission via the n = 0 as well as the n = 1 mode . The n = 1 mode is not directly disturbed, but if the n = 0 and n = 1 modes overlap (in ω^2/ω_p^2) there is interference. From this experiment it is apparent that coupling from dipole fields to rotational mode and vice versa can take place in the presence of this weak magnetic field. Transmission measurements performed in a magnetically shielded box showed no extraneous coupling. In these measurements there is always some coupling to both modes because of imperfect symmetry in the couplers.

The strong influence of the earth's magnetic field is quite astounding as its value, 1/2 Gauss, corresponding to an electron gyrational frequency of 5 Mcps is very small compared to the measuring frequency, here 1700 Mcps. The effect observed in the waveguide experiment, is probably the same observed by

Messiaen and Vandenplas[21].

The rotationally symmetric mode also influences cavity measurements such as often used to determine electron density and collision frequency[13]. The Q value of a cavity excited in the TM_{010} mode shows sharp minima at electron densities corresponding to those for propagation of the n = 0 mode at the probing frequency. The Q value of a cavity being tested in transmission can easily be determined by observing the 1/2 power points of transmission. If, however, the generator output is reasonably constant, a measure of the Q value is the amplitude of the transmitted signal. Figure 10 shows the experimental arrangement and the transmitted signal as a function of discharge current for many discrete probing frequencies. The values of ω^2/ω_p^2 corresponding to minima in the transmitted signal are those for propagation of the different bands of the n = 0 mode at the appropriate r_w^2/λ_d^2's. (The minimum at $\omega^2/\omega_p^2 = 0.3$ is thought to be associated with the lowest dipole resonance) This is not surprising as the electric field in the cavity is not completely axial due to holes in the end surfaces through which the tube extends. The cavity acts then as an n = 0 coupler whose "gap" is very large. Energy may then be coupled out of the microwave cavity and transmitted along the column or dissipated by collisional or Landau damping.

A final experiment which will be reported here demonstrates a dependence between the so called "high frequency probe" (h.f. probe) measurements and the transmission modes. A copper tube with a coaxial connector, see Figure 3d, is placed on the discharge tube and connected to a generator and a recorder as shown in Figure 11a. Figure 11b shows the voltage of the probe as a function of discharge current with the microwave generator turned on and turned off. There are no nonlinear components in the external circuit. The peaks in the rectified microwave current namely the sharp voltage minima are also plotted in Figure 6. The striking correlation between the h.f. probe resonance points and the cutoff points of the n = 1 and n = 0 modes suggests that longitudinal wave propagation is related to these h.f. probe re-

sonances. Since these waves are not confined to the region immediately surrounding the probe, one would infer that it is necessary to consider the entire plasma when evaluating probe measurements.

Theory

A discussion of the theory of these modes of propagation may be introduced by briefly reviewing a few of the relevant papers dealing with isotropic plasmas. W.O. Schuman[22] and associates, Hahn[23], Ramo[24], Trivelpiece and Gould[25], and others have discussed solutions to Maxwell's equations for a bounded cold ($T_e = 0$) plasma. The plasma itself is characterized in these cases by an index of refraction, $n^2 = 1 - \frac{\omega_p^2}{\omega^2}$ or a dielectric constant $\varepsilon = \varepsilon_o \left(1 - \frac{\omega_p^2}{\omega^2}\right)$. It is shown in these papers that a solution of the electromagnetic equations exists for a bounded plasma for which there is propagation along the column with wavelengths much shorter than the vacuum wavelength. In the paper by Trivelpiece and Gould[25] a quasi-static approximation, $E = -\text{grad}\phi$, is assumed. E is the electric field vector and ϕ a scalar potential. The resulting equation, $\text{div}\,\varepsilon\,\text{grad}\,\phi = 0$, along with appropriate plasma-glass boundary conditions is solved. One solution for a band of propagation with rotationally symmetry and one for a band with dipole symmetry are found. These solutions are clearly identificable with the lowest $n = 0$ band (with cutoff frequency $\omega^2/\omega_p^2 = 0$) and with the lowest $n = 1$ band which exhibits the strong backward wave characteristic. Although these solutions predict the main properties of these modes many aspects are not included.

In the paper by PNG[4] the effects of a non-zero electron temperature and an inhomogeneous plasma are taken into account in the discussion of the cutoff dipole resonances. The basic analytical approach used by PNG[4] in a simplified form, will be used throughout most of this treatment.

The basic equations, which will be used to describe the hot plasma are those derived for the two fluid model by Schlüter[26]. These equations can also be derived as an approximation (velocity moments) to the Boltzmann equation. The following approximations are made:

The plasma is considered to be at rest (zero order).
Collisions are considered negligible.
Ions are considered to remain identically at rest (zero and first order).
A uniform isotropic electron temperature T_e is assumed (henceforth the subscript on T_e will be omitted).
A pertubation pressure term of the form $p_1 = 3\,kTn_1$, is assumed.

$$\frac{\partial n_e}{\partial t} = -\nabla\cdot(n_e \underset{\sim}{v}_e) \qquad \text{equation of continuity} \qquad (5)$$

$$m_e n_e\left(\frac{\partial \underset{\sim}{v}_e}{\partial t} + (\underset{\sim}{v}_e\cdot\nabla)\underset{\sim}{v}_e\right) = -e n_e \underset{\sim}{E} - \nabla p_e \qquad \text{momentum equation} \qquad (6)$$

$$\nabla p_e = \gamma K T \nabla n_e \qquad \text{gas law} \qquad (7)$$

The quantities n_e, $\underset{\sim}{v}_e$ and p_e are the electron density, velocity and pressure respectively, K is the Boltzmann constant and γ_1 is the ratio of the specific heat at constant pressure to that at constant volume. $\underset{\sim}{E}$ is the electric field vector, e is the magnitude of the electron charge.

Maxwell's equations are approximated by considering the electric field vector derivable from a scalar potential.

$$\underset{\sim}{E} = -\nabla\phi \qquad (8)$$

$$\nabla^2\phi = \frac{e(n_e - n_i)}{\varepsilon_0} \qquad (9)$$

$n_i = n_i(r)$ is the ion density.

This quasi-static approximation is applicable where the dimensions involved are small compared with the vacuum wavelengths of the impressed signals; the dimensions involved are generally of the order of a few centimeters whereas the vacuum wavelengths are of the order of 100 centimeters. The quasistatic approximation becomes invalid at the highest measuring frequencies used (4000 Mcps or λ_o = 7.5 cm). Most of the measurements, however, were made at frequencies between 50 and 2000 Mcps.

A zero order (time independent) and first order (perturbation) dependence of the variables is assumed:

$$\left.\begin{aligned} n_e &= n_{eo}(r) + n_{e1}(r,t) \\ n_i &= n_{io}(r) \\ \phi &= \phi_o(r) + \phi_1(r,t) \\ \underset{\sim}{v}_e &= 0 + \underset{\sim}{v}_{e1}(r,t) \\ p_e &= p_{eo}(r) + p_{e1}(r,t) \\ \underset{\sim}{E} &= \underset{\sim}{E}_o(r) + \underset{\sim}{E}_1(r,t) \end{aligned}\right\} \quad (10)$$

Assuming a $e^{i\omega t}$ time dependence the zero and first order equations are respectively:

$$0 = 0 \quad (5a)$$

$$i\omega n_{e1} = -\nabla\cdot(n_{eo}\underset{\sim}{v}_{e1}) \quad (5b)$$

$$0 = -e n_{eo}\underset{\sim}{E}_o - \nabla p_{eo} \quad (6a)$$

$$m_e n_{eo} i\omega \underset{\sim}{v}_{e1} = -e(n_{eo}\underset{\sim}{E}_1 + \underset{\sim}{E}_o n_{e1}) - \nabla p_{e1} \quad (6b)$$

$$\nabla p_{eo} = \gamma_o KT \nabla n_{eo} \qquad \gamma_o = 1 \qquad \text{(perfect gas law)} \quad (7a)$$

$$\nabla p_{e1} = \gamma_1 KT \nabla n_{e1} \qquad \gamma_1 = 3 \qquad \text{(one dimensional adiabatic compression; see discussion below)} \quad (7b)$$

$$\underset{\sim}{E}_o = -\nabla\phi_o \quad (8a)$$

$$\underset{\sim}{E}_1 = -\nabla\phi_1 \quad (8b)$$

$$\nabla^2\phi_0 = \frac{e(n_{e0}-n_{i0})}{\varepsilon_0} = -\nabla\cdot\underset{\sim}{E}_0 \qquad (9a)$$

$$\nabla^2\phi_1 = \frac{e\,n_{e1}}{\varepsilon_0} = -\nabla\cdot\underset{\sim}{E}_1 \qquad (9b)$$

As the electron collision frequencies are generally seveal orders of magnitude less than the impressed frequencies one may consider the wave motion as adiabatic. Through the linearisation of the adiabatic law, $\frac{d}{dt}\left(\frac{p}{n^\gamma}\right)=0$, one obtains for the first order pressure term,

$$p_1 = 3KT n_1 + \frac{2KT}{i\omega}\,\underset{\sim}{v}_1\cdot\nabla n_0$$

The value of γ is taken as 3 as the wave motion is considered to be a one dimensional adiabatic compression. The second term on the right handside complicates the calculation very considerably and one would like to see if it may be neglected. Obviously it is zero in the case of an homogeneous plasma. When an inhomogeneous profile is considered, ∇n_0 has only a radial component and the troublesome term disappears for the cylindrically symmetric mode as the wave propagation (e.g. $\underset{\sim}{v}_1$) becomes essentially parallel to the axis of the discharge. Only the cylindrically symmetric mode with its radial and axial components of the first order variables will be considered in the inhomogeneous calculations. One may attempt to judge the importance of this term by building the quotient, Q, of the first term on the right hand side divided by the second.

$$Q = \frac{3KT n_1 i\omega}{2KT\,\underset{\sim}{v}_1\cdot\nabla n_0} = -\frac{3KT(\underset{\sim}{v}_1\cdot\nabla n_0 + n_0\nabla\cdot\underset{\sim}{v}_1)}{2KT\,\underset{\sim}{v}_1\cdot\nabla n_0} = -\frac{3}{2}\left(1+\frac{n_0\nabla\cdot\underset{\sim}{v}_1}{\underset{\sim}{v}_1\cdot\nabla n_0}\right)$$

Here use has been made of continuity equation. If the $|Q|$ can be shown to be large compared to unity then neglect of this term is justified. In part two of Appendix III a calculation of Q is given for the profile to be discussed in Case C. It is seen that Q is negligible under most but not all conditions. As an indication of the importance of this term one may reflect on the excellent agreement between theory and experiment obtained by PNG[4] where the first order pressure term is assumed equal to 3 kT n_1.

In further calculations p_1 will be set equal to $3kT\, n_1$. In particular, the manner in which the neglected term would influence the boundary conditions calculated in appendix II is not investigated.

It may be remarked, that by taking velocity moments of the Boltzmann equation, and terminating with the setting to zero of the heat flow tensor, yields the following expression for the j component of the grad p_1 term ($p_o = kT\, n_o$):

$$(\nabla p_1)_j = 3KT \frac{\partial n_1}{\partial x_j} + \frac{KT}{i\omega} \sum_{k=i,j,k} \frac{\partial}{\partial x_k} \left(-n_o \frac{\partial v_j}{\partial x_k} + 2 v_k \frac{\partial n_o}{\partial x_j} + n_o \frac{\partial v_k}{\partial x_j} \right)$$

This expression is not equal to that obtained from the adiabatic law. If, however, one considers the special case of a plane longitudinal wave propagating in an inhomogeneous medium with the E-field vector parallel to grad n_o one obtains for the component of grad p_1 in the propagation direction (index I),

$$(\nabla p_1)_I = 3KT \frac{\partial n_1}{\partial x_I} + \frac{2KT}{i\omega} \frac{\partial}{\partial x_I} \left(v_I \frac{\partial n_o}{\partial x_I} \right) .$$

In this special case the moment equation approximation and the adiabatic law yield the same result.

If one takes the divergence of the first order momentum equation, (6b), one obtains after combination with the other equations

$$0 = (\nabla^2 + k^2) \nabla^2 \phi_1 - \left[\frac{\nabla \phi_1 \cdot \nabla \omega_p^2}{c_s^2} + \frac{1}{3} \frac{\nabla^2 \omega_p^2}{\omega_p^2} \nabla^2 \phi_1 \right. \qquad (11)$$

$$\left. - \frac{1}{3} \left(\frac{\nabla \omega_p^2}{\omega_p^2} \right)^2 \nabla^2 \phi_1 + \frac{1}{3} \frac{\nabla \omega_p^2}{\omega_p^2} \cdot \nabla (\nabla^2 \phi_1) \right]$$

where

$$c_s^2 \equiv \frac{3KT}{m_e} \qquad (12)$$

$$k^2 \equiv \frac{\omega^2-\omega_p^2}{c_s^2} \quad \text{and} \quad \omega_p^2 \equiv \omega_p^2(r) \equiv \frac{n_{e0}(r)\,e^2}{\varepsilon_0 m_e} \,. \tag{13}$$

At this point it is judicious to discuss equation (11) and the plausibility of using the approximate equations (5), (6) and (7). In the case of an homogeneous plasma the entire bracketed term in (11) disappears and one may consider the quantity k^2 of equation (13) to be the square of the wave vector of a longitudinal wave. Equation (13), so interpreted, then is the dispersion relation for a longitudinal wave in an infinite homogeneous plasma and is equivalent to the index of refraction given in (2). The thus simplified equation (11) then represents the wave equation for longitudinal and "transverse" waves. The possibility of pure transverse wave is excluded through the quasistatic approximation of Maxwell's equations. The value of the approximation of the Boltzmann equation, which equations (5), (6) and (7) constitute, is difficult to estimate in the case of an inhomogeneous plasma. The approximation does not include Landau damping. One may, however, consider, as an initial indication of the range of applicability, a comparison of ω^2/ω_p^2 calculated from (13), with $(\omega^2/\omega_p^2)'$, as obtained through numerical solution of the Boltzmann equation in an homogeneous medium. (Here k is assumed real and $(\omega^2/\omega_p^2)'$ is the real part of complex frequency) In Table I a value k is assumed and the value of ω/ω_p from equation (13) is given and the value of $(\omega/\omega_p)'$ as obtained from numerical solution of the Boltzmann equation[27]. For large values of $kc_s/\sqrt{3}\,\omega_p$ the imaginary part of ω/ω_p, calculated from the Boltzmann equation, becomes very large.

Table I

$\frac{kc_s}{\sqrt{3}\,\omega_p}$	$\frac{\omega}{\omega_p}$	$(\frac{\omega}{\omega_p})'$
1	2	1.9
2	3.6	3.2
3	5.3	4.0
4	7.0	5.2
5.8	10.0	6.8
9	15.6	10
15	26.0	16

From this table it is seen that for ω/ω_p smaller than, say, 10 the error in k is less than 35%. The comparison does not, of course, reflect on any of the terms in the brackets in (11) and also neglects the imaginary part of ω/ω_p.

It is now also propitious to discuss the methods of solution of equation (11). In an earlier paper[28] the direct numerical integration of (11) for a particular previously calculated electron profile i.e. $n_{eo}(r)$ or $\omega_p^2(r)$ is given. Quite good agreement between the calculated and measured ω-β curves is noted in this paper. In the present paper three approximations of the electron profile will be made and analytical solutions of (11) will be given. The method of solution used in reference 28 will also be discussed.

Primary emphasis will be given the rotationally symmetric mode because it is inherently simpler and because of the existance of calculations for the dipole mode[4)28)].

These approximations are:

A The plasma will be assumed homogeneous. This solution is instructive and has some applications for tenuous plasmas, that is, where $r_w^2/\overline{\lambda_d^2} \lesssim 100$. At large values of $\overline{\lambda_d^2}$ wave action takes place over a significant portion of the tube[4)].

B The plasma will be assumed composed of two regions, one, a homogeneous core and, two, a homogeneous region between the core and glass wall. This solution is algebraically more complicated than A but has application over a wide range of electron profiles.

C The plasma will be characterized by a sheath whose thickness is small compared to the tube radius. A particular functional dependence for the sheath will be assumed and, after a change from cylindrical coordinates to cartesian, a solution of the wave equation will be found. (The change of coordinates used here is similar to that often used when discussing the skin effect in cylindrical conductors) The solution found here has application only for large values of $r_w^2/\overline{\lambda_d^2}$ namely for relatively thin sheaths and is valuable as an asymptotic presen-

tation.

The methods of solution, A, B, and C, consist of approximating the electron density profile with functions which allow analytical solution in terms of known functions. One may expect the theoretical results to best agree with observation when the profiles are used which exist in the plasma. In paper 28 the result of such a calculation is shown. Equation (11) is solved numerically for electron profiles calculated by Parker[17]. The method of calculation is described in the paper by PNG[4]. This calculation, which has only been carried out for the dipole mode, shows good agreement with observation.

The zero order radial electron density profiles, that is n_{eo}, for a collisionless plasma with cylindrical symmetry shown in Figure 12 have been reproduced from Parker's[17] work. The density $n_{eo}(r)$ is normalized to the density at the center of the tube, $n_{eo}(0)$, which in turn may be related to the average density $\overline{n_{eo}}$. The radius is normalized to the radius of the plasma column, r_w.

For high density plasmas, small values of the average squared Debye length $\overline{\lambda_d^2}$, there is a clear sheath formation near the glass wall. However, for thin plasmas there is no clearly defined sheath. It was shown[4] that most of the wave action, for the lower bands, takes place in the region of the sheath, if one is present, and otherwise over most of the tube.

Henceforth the index 1 will only be included where it is necessary for clarity.

Case A:

For the case of a homogeneous plasma equation (11) simplifies to

$$(\nabla^2 + k^2)\nabla^2\phi = 0 \qquad (14)$$

Since k is now not a function of r, (14) reduces (for $k^2 \neq 0$) to two second order differential equations for which we assume the dependence $\phi(r,\theta,z) = R(r)\, e^{i\beta z}\, e^{in\theta}$.

Rotationally symmetric mode:

$$\frac{\partial^2 R(r)}{\partial r^2} + \frac{1}{r}\frac{\partial R(r)}{\partial r} - \beta^2 R(r) = 0 \qquad \text{(follows from } \nabla^2\phi = 0\text{)} \qquad (14a)$$

$$\frac{\partial^2 R(r)}{\partial r^2} + \frac{1}{r}\frac{\partial R(r)}{\partial r} + (k^2 - \beta^2) R(r) = 0 \qquad \text{(follows from } (\nabla^2 + k^2)\phi = 0\text{)} \qquad (14b)$$

The general solution of (14a) is a linear combination of $I_o(\beta r)$ and $K_o(\beta r)$ and of (14b) a linear combination of $Y_o(k_e r)$ and $J_o(k_e r)$ for $k_e^2 > 0$ and a combination of $K_o(k_e r)$ and $I_o(k_e r)$ for $k_e^2 < 0$. One often considers k_e as the component of the propagation vector perpendicular to the tube axis and β as the component parallel to the axis.

$$k_e^2 \equiv k^2 - \beta^2 \qquad k_e \equiv +\left(|k^2 - \beta^2|\right)^{\frac{1}{2}} \qquad (15)$$

The solution of (14a) gives the potential ϕ also outside the plasma as the equation $\nabla^2\phi = 0$ holds everywhere. All K_o and Y_o solutions <u>inside</u> the plasma and I_o solutions <u>outside</u> the plasma must be disregarded because of singularities at the origin and at infinity respectively. The solution is then:

$$R_{(r)}^{\text{interior}} = c_1 J_o(k_e r) + c_2 I_o(\beta r)$$

$$R_{(r)}^{\text{exterior}} = c_3 K_o(\beta r) \qquad (16)$$

The case $k_e^2 > 0$ is treated now, for $k_e^2 < 0$ proper substitutions must be made. The sign of k_e^2 directly effects only the solutions of the "longitudinal wave equation". For the case k_e^2 larger than zero, one has an oscillating solution, $J_o(k_e r)$; for k_e^2 negative one has an evanescent solution ($I_o(k_e r)$; is exponential in nature).

Plasma-Glass Boundary Conditions:

The following boundary conditions are taken at r_w:

α) The boundary is considered reflecting for the particles, thus the radial component of v_{el} is zero here.
It follows then from (6b) through (9b) that

$$0 = \frac{\omega_p^2}{c_s^2}\frac{\partial \phi}{\partial r}^{\text{interior}} - \frac{\partial \nabla^2\phi}{\partial r}^{\text{interior}}\Bigg|_{r=r_w} . \qquad (17)$$

β) From $\nabla \cdot \varepsilon E = 0$ (surface charges are precluded by α)) we have

$$\varepsilon^i \frac{\partial \phi^i}{\partial r} = \varepsilon^e \frac{\partial \phi^e}{\partial r}\Bigg|_{r=r_w} . \qquad \varepsilon^i \equiv \varepsilon_o \text{ (vacuum)} \qquad (18)$$

$$\frac{\varepsilon^e}{\varepsilon^i} \equiv \kappa^R$$

κ^R is the equivalent relative dielectric constant, for the rotationally symmetric mode, of the glass discharge tube and air surrounding the plasma, see Appendix I. The dielectric constant in the plasma, ε^i, is, of course, that of vacuum as the electric charges are considered explicitly.

γ) From the equation $E = -\nabla\phi$ it follows curl E = 0 and we have

$$\phi^i(r_w) = \phi^e(r_w) . \qquad (19)$$

Equation (19) follows also by requiring curl E to be finite.

One of the three arbitrary constants of (16) may be chosen to be 1. The application of the boundary conditions α, β, and γ then yields the dispersion equation

$$\frac{\omega_p^2}{\omega^2} - 1 = \kappa^R \beta r_w \frac{K_1(\beta r_w)}{K_o(\beta r_w)} \left(\frac{\omega_p^2}{\omega^2} \frac{J_o(k_e r_w)}{k_e r_w J_1(k_e r_w)} + \frac{I_o(\beta r_w)}{\beta r_w I_1(\beta r_w)} \right) . \qquad (20)$$

For the case $k_e^2 < 0$ the following substitutions are to

be made in equation (20): $J_o(k_e r_w) \rightarrow I_o(k_e r_w)$ and $J_1(k_e r_w) \rightarrow -I_1(k_e r_w)$

The solution to (20), which was obtained by a computer, may be conveniently represented by two plots. One plot gives the cutoff values, $(\omega^2/\omega_p^2)_{co}$, versus r_w^2/λ_d^2, Figure 13, and the other the ω-β diagram for several values of r_w^2/λ_d^2, Figure 14, 15 and 16. There exists an unlimited number of solutions to (20) for $\omega^2 > \omega_p^2$ due to the oscillatory property of the J function but only one solution for $\omega^2 < \omega_p^2$. This follows from the exponential nature of the I (and K) functions.

The relationship between r_w^2/λ_d^2 and the other parameters, ω^2/ω_p^2 and βr_w, is clearly shown in equation (21), which is another form of equation (13).

$$\frac{\omega^2}{\omega_p^2} = 1 + 3\frac{\lambda_d^2}{r_w^2}\left(k_e^2 r_w^2 + \beta^2 r_w^2\right) \qquad \left(\text{For Case A } \overline{\omega_p^2} \equiv \omega_p^2\right) \qquad (21)$$

An investigation of the cutoff values, $(\omega^2/\omega_p^2)_{co}$, that is, $\beta = 0$ or $k_e^2 = k^2$ of equation (20) may be made by use of the asymptotic expansions of the I and K functions. It is, however, simple to solve for this case by starting with equations (14a) and (14b). The radial part, R(r), of the solution of "the electromagnetic part", is equal to a constant and logarithm of r. The logarithm solution must be disregarded in the plasma as well as outside because of singularities. The constant may be conveniently chosen to be zero outside the plasma, that is $\phi^e = 0$. The solution of the "longitudinal wave part" $(\nabla^2 + k^2)\,\phi = 0$ is either $J_o(k_e r)$ or $I_o(k_e r)$ depending on the sign of k^2.

The potential is then:

$$\left.\begin{aligned} \phi^i &= a_1 J_o(k_e r) + a_2 \qquad \left(\text{or } J_o(k_e r) \rightarrow I_o(k_e r)\right) \\ \phi^e &\equiv 0 \end{aligned}\right\} \beta = 0$$

An application of the boundary conditions α, β and γ leads to the dispersion equation

$$J_1(k_e r_w) = 0 \qquad \text{for } k_e \neq 0 \qquad (22)$$

Solution of (22) yields the values of k_e which correspond to cutoff and, when combined with (21), gives $(\omega^2/\omega_p^2)_{co}$. Two exceptional cases, $\omega^2 = \omega_p^2$ and $\omega^2 = 0$, should be investigated

In case of $\omega^2 = \omega_p^2$ (or $k^2 = 0$) one must solve the equation $\nabla^2\nabla^2\phi = 0$. For the conditions in question, n = 0 mode and $\beta = 0$, one obtains the general solution of the differential equation as:

$$\phi = a_1 + a_2 \ln(r) + a_3 r^2 + a_4 r^2 \ln(r)$$

Because of the singularly at the origin, a_2 must be set equal to zero. Chosing the potential outside the plasma again equal to zero one obtains, after application of boundary conditions α, β, and γ, the trivial solution $a_1 = a_3 = a_4 = 0$. The other case $\omega^2 = 0$ corresponding to $k_e^2 = \frac{0 - \omega_p^2}{c_s^2}$ also leads to a trivial solution. Here k_e^2 is negative so that one must choose $I_o(k_e r)$ as mathematical solution of the "longitudinal wave equation", (14b), in place of $J_o(k_e r)$. The boundary condition of the continuity of $\epsilon \frac{\partial \phi}{\partial r}$ then requires that the derivative of $I_o(k_e r)$ be zero ($\phi^e = 0$) which can only be satisfied by $k_e = 0$ which in turn states that $\omega_p^2 = 0$ or no plasma. A physical discussion of these cases follows.

The fact that there is no field outside the plasma at cutoff follows from the symmetry involved. In the quasistatic approximation, "lines of electric field" must begin and end on charges of opposite sign. Since there is no variation in either θ or z, should there appear a charge somewhere on the surface of the plasma it must appear everywhere on the surface. This means that the "electric field lines" could not terminate. Another statement of this is that the net charge in a volume of arbitrary length formed by cutting the discharge tube at right angles to its axis must be zero due to the conservation of charge. (Because of rotational symmetry the end surfaces may be segments of the cross section). Should this not be true, at one time at all points along the tube (because of no variation in z at cutoff) there would appear e.g. an E field directed outward and one half period later one directed inward. This violates the conservation of

charge. Note, however, that this condition need not hold when there is propagation in the z direction. This cutoff condition, of no external field, can be shown to hold through direct integration of the charge density. For these reasons it is clear that no solution exists for $\omega^2 = 0$. (Here for the case of $\omega^2 < \omega_p^2$ the solution of the equation $(\nabla^2 + k^2)\,\phi = 0$ is an I_o function and the charge density is obtained through $\nabla^2\phi = -\frac{e n_{e1}}{\varepsilon_o}$. Integration of the charge density in the radial direction is then, except for constants, the integration of $I_o(k_e r) r\,dr$ which cannot yield zero for $r_w > 0$; $I_o(x) > 0$.) The band of propagation, for which $\beta \to 0$ as $\omega^2/\omega_p^2 \to 0$, however, does not exist as long as β is not identically zero. This band, analized from the standpoint of a cold plasma, is discussed by Trivelpiece and Gould[25] and others.

This analysis of the n = 0 mode for a homogeneous plasma has disclosed the following facts:

There is only one solution to the dispersion equation for $\omega^2 < \omega_p^2$.

There are infinitely many solutions for $\omega^2 > \omega_p^2$. At cutoff there is no solution for $\omega^2 = \omega_p^2$.

The solution for k^2 at cutoff is $J_1(k_e r_w) = 0$ $(k_e \neq 0)$. There is no field outside the plasma at cutoff (a consequence of the symmetry) and therefore no direct detection at cutoff with the present methode of observation is possible.

Dipole Mode

Starting with equation (14) and assuming $\phi\,(r,\theta,z) = R(r)e^{i\theta}e^{i\beta z}$ a similar analysis of the dipole mode can be carried out. The general dispersion equation for $k_e^2 > 0$ is then

$$\left(\frac{\omega_p^2}{\omega^2}-1\right)\left[\frac{I_1(\beta r_w)}{\beta r_w I_o(\beta r_w)}-1\right]\left[1-\frac{J_1(k_e r_w)}{k_e r_w J_o(k_e r_w)}\right] = K^D\left[\frac{\omega_p^2}{\omega^2}\left(\frac{I_1(\beta r_w)}{\beta r_w I_o(\beta r_w)}-1\right)\frac{J_1(k_e r_w)}{k_e r_w J_o(k_e r_w)} + \left(1-\frac{J_1(k_e r_w)}{k_e r_w J_o(k_e r_w)}\right)\frac{I_1(\beta r_w)}{\beta r_w I_o(\beta r_w)}\right]\left[-\frac{\beta r_w K_o(\beta r_w)}{K_1(\beta r_w)}-1\right] \quad . \tag{23}$$

κ^D is defined similarly to κ^R , (19), but for the dipole mode, see also Appendix I. For the case $k_e^2 < 0$, similar substitutions must be made: $J_o(k_e r_w) \rightarrow I_o(k_e r_w)$ and $J_1(k_e r_w) \rightarrow I_1(k_e r_w)$.

The equation for the cutoff condition which is also reasonably complicated will not be given here (it is given by PNG[4]). The dipole mode also possesses one propagation band for $k_e^2 < 0$ which, however, has a non-zero value of $(\omega^2/\omega_p^2)_{co}$. All bands have fields outside the plasma at cutoff because of the dipole configuration. The lowest band of propagation has also been analized[25] from the standpoint of a cold plasma. The first n = 0 and n = 1 bands are, however, the only bands which the cold plasma analysis yields.

A plot of the cutoff points of the dipole mode is given in Figure 17. The cutoff values for the dipole mode obtained through direct solution of equation (11) is given by PNG[4]. Figures 18, 19, and 20 give ω-β curves for the dipole mode calculated from (23).

Case B:

In the model to be discussed the electron density is assumed to change as a function of radius. In the region between radius zero and r_1, region A, it shall have the value corresponding to $\omega_{p_A}^2$ and in region B, radius between r_1 and r_w, the value $\omega_{p_B}^2$, in accordance with the physical profiles, is always less than $\omega_{p_A}^2$. The discontinuity is introduced as a means of approximating the electron density profile. Only the n = 0 mode will be considered here.

Table II

Region	A	B	Exterior
Radius	$0 \leq r < r_1$	$r_1 \leq r < r_w$	$r_w \leq r$
$\nabla^2\phi = 0$ >	$R(r) = c_1 I_o(\beta r)$	$R(r) = c_3 I_o(\beta r) + c_4 K_o(\beta r)$	$R(r) = c_7 K_o(\beta r)$
$(\nabla^2 + k^2)\phi = 0$ >	$+ c_2 I_o(k_a r)$	$+ c_5 J_o(k_b r) + c_6 Y_o(k_b r)$	———
Where	$k_A^2 \equiv \frac{\omega^2 - \omega_{pA}^2}{c_s^2}$	$k_B^2 \equiv \frac{\omega^2 - \omega_{pB}^2}{c_s^2}$	———
Assumed is	$k_A^2 - \beta^2 < 0$	$k_B^2 - \beta^2 > 0$	———
With	$k_a = +(\lvert k_A^2 - \beta^2 \rvert)^{\frac{1}{2}}$	$k_b = -(\lvert k_B^2 - \beta^2 \rvert)^{\frac{1}{2}}$	———

In cases where the signs of $k^2_{A,B} - \beta^2$ are other than those assumed appropriate changes of functions must be made (this is done in the computer program).

Boundary Conditions

The boundary conditions at the plasma-glass boundary, $r=r_w$ are those previously given, namely α, β and γ.

The boundary conditions at the point of the electron density discontinuity have been calculated from the basic equations, (5) to (9). (See Appendix II)

These boundary conditions for $r = r_1$ are:

δ) The continuity of the potential,

$$\phi_A = \phi_B \,. \tag{24}$$

ε) The continuity of the radial components of the electric field, (the dielectric constant is that of vacuum),

$$\frac{\partial \phi_A}{\partial r} = \frac{\partial \phi_B}{\partial r} \,. \tag{25}$$

The continuity of the tangential components of the electric field is assured by (24) as all derivatives in the axial direction can be replaced by $i\beta$.

ϛ) The continuity of the radial components of current,

$$\frac{\omega_{pA}^2}{c_s^2}\frac{\partial \phi_A}{\partial r} - \frac{\partial(\nabla^2\phi_A)}{\partial r} = \frac{\omega_{pB}^2}{c_s^2}\frac{\partial \phi_B}{\partial r} - \frac{\partial(\nabla^2\phi_B)}{\partial r} \,. \tag{26}$$

The equation (27) for the current, $\underset{\sim}{j}$, was obtained through combination of equations (5b) to (9b).

$$\underset{\sim}{j} = -e n_{e0} \underset{\sim}{v}_{e1} = \frac{\varepsilon_0 c_s^2}{i\omega}\left(-\frac{\omega_p^2}{c_s^2}\nabla\phi_1 + \nabla(\nabla^2\phi_1)\right) \tag{27}$$

η) The second derivative of ϕ is discontinuous,

$$\frac{\partial^2 \phi_B}{\partial r^2} = \left(\frac{\omega_{pB}^2}{\omega_{pA}^2}\right)^{\frac{1}{3}} \frac{\partial^2 \phi_A}{\partial r^2} + \beta^2 \phi_A \left(1 - \left(\frac{\omega_{pB}^2}{\omega_{pA}^2}\right)^{\frac{1}{3}}\right) . \qquad (28)$$

Equation (28) is equivalent to the relation $\frac{n_{1A}}{(\omega_{pA}^2)^{\frac{1}{3}}} = \frac{n_{1B}}{(\omega_{pB}^2)^{\frac{1}{3}}}$.

The continuity of the radial components of the electric field and the current show that no surface charge is present at the discontinuity.

The choice of r_1, ω_{pA}^2 and ω_{pB}^2 was made in manner appropriate to the electron profiles calculated by Parker[17] and shown in Figure 12. Reference to those profiles shows that, for large values of $r_w^2/\bar{\lambda}_d^2$, a sharp change in the distribution function takes place at $n(r) = 0.35\ n(0)$. The position of the discontinuity, r_1, was chosen so that $n(r_1) = 0.35\ n(0)$. The density in region B was chosen as one half that at the discontinuity, namely $n_B = 0.175\ n(0)$. Since all experimental work is referenced to the average density $\bar{n}$ the value of the function $N = \frac{\bar{n}}{n(0)}$ is taken from Parker's work[17]. The plasma density n_B or plasma frequency (squared) ω_{pB}^2 can now be related to the average, over the entire tube cross section, of the square of the plasma frequency.

$$\frac{\omega_{pB}^2}{\bar{\omega}_p^2} = \frac{0.175}{N}$$

The value of $\omega_{pA}^2/\bar{\omega}_p^2$ was then adjusted so that the average densities of the profile according to Parker and the approximation are equal, that is,

$$\pi r_1^2 \omega_{pA}^2 + \pi (r_w^2 - r_1^2) \omega_{pB}^2 = \pi r_w^2 \bar{\omega}_p^2 .$$

For greater computional ease, analytical formulae were developed from Parker's data for N and r_1/r_w as a function of $r_w^2/\bar{\lambda}_d^2$ which is the only parameter needed to determine the profiles. $r_w^2/\bar{\lambda}_d^2$ is abbreviated with P.

$$N \cong 0.341 \log_{10} P - 0.0297 (\log_{10} P)^2 - 0.311$$

$$r_1/r_w \cong -\frac{0.753}{\log_{10}P} + \frac{0.10}{(\log_{10}P)^2} - \frac{3.705}{P^{1/2}} + \frac{15.4}{P} + 1.1080$$

Seven homogeneous equations for the c_1, c_2 ... c_7 result from the boundary conditions $\alpha, \beta, \ldots, \eta$. In order that these seven homogeneous equations have a solution, the determinant of the seven x seven matrix of these equations must be zero. The elements are coefficients of the c_1, c_2 ... c_7 terms resulting from the boundary conditions.

The values of $\omega^2/\overline{\omega_p^2}$ which solve this determinant are shown in Figure 13, $(\omega^2/\overline{\omega_p^2})_{co}$ vs $r_w^2/\overline{\lambda_d^2}$ and 14, 15, 16, $\omega - \beta$ curves.

One sees a significant improvement in the agreement with the measurement for the lower bands. From Figure 13 one notices, however, at large values of $r_w^2/\overline{\lambda_d^2}$ a behavior similar to that in Case A. Namely, that the bands lie close to one an other when propagation can take place over the entire cross section of the tube ($k_A^2 > 0$).

Calculations for parameter values of $r_w^2/\overline{\lambda_d^2}$ larger than 10^4 could not be carried out for Case B as arguments of I functions of the order of 100 appeared and function values are too large for the computer.

Case C:

Before beginning with a discussion of this model it will be helpful to discuss some of the salient features of the analysis performed on these modes. In particular, as will be shown below, the lowest band of propagation of the rotationally symmetric mode requires consideration of both longitudinal and electromagnetic waves in order to predict correctly its dispersion curve. Many aspects of the upper bands of this mode are, however, reasonably accurately predicted when one considers only longitudinal waves. The part of the dispersion curve for the lowest band in the region of small β is well described by considering only the e-m wave, (i.e. $T_e = 0$), but the existence of a maximum value of $\omega^2/\overline{\omega_p^2}$ beyond which there is no transmission[25] is contrary to experimental observations. An analysis including

the plasma waves shows the propagation at large β to be similar to that for the higher bands, (Figures 14, 15, 16) i.e. no termination for increasing ω^2/ω_p^2. Consideration of only the plasma wave, however, completely fails to show this lowest band.

Turning attention to the higher bands, for an homogeneous plasma, an analysis based only on the longitudinal or plasma waves assumes to equation $(\nabla^2 + k^2)\,\phi = 0$. This equation possesses only one non singular solution and consequently only one boundary condition is appropriate. A most reasonable condition would be that of reflecting glass walls, namely, the radial component of velocity, or current, equal to zero at r_w. For pure plasma waves the current is proportional to the electric field and therefore there would exist no external electric field. Although this fact is contrary to experiment (no coupling would be possible) it none the less represents a good approximation to the boundary conditions as far as the dispersion relation is affected. Using the notation introduced in Case A, one obtains, considering only plasma waves, the general dispersion equation, valid for propagation and cutoff,

$$J_1(k_e r_w) = 0 \qquad (29)$$

It is immediately obvious that this equation is identically equal to equation (22) in Case A for cutoff. The solution of equation (29) for $\beta \neq 0$ differs slightly from the solution of Case A given in Figures 14, 15, and 16. The forgoing discussion yields credulance to the hypothesis assumed in Case C, namely, that the higher bands of propagation in an inhomogeneous plasma approximately can be described by considering only longitudinal waves. This hypothesis has also been stated by Weissglas[29].

As is seen in Figures 13 and 17 the homogeneous approximation of the plasma is quite unsatisfactory for large r_w^2/λ_d^2. Gould[30] stated, then with reference to the dipole case, that attention to the inhomogeneous electron profile would probably yield results in agreement with observation. In the paper by PNG[4] it is shown that, for large r_w^2/λ_d^2, the wave action for the lower dipole bands at cutoff is quite confined to the sheath

region. The problem to be discussed now, is that of solving the wave equation in the sheath region of the plasma. Two geometrical approximations will be made, first, as the thickness of the sheath is small compared to the radius, the cylindrical coordinates will be exchanged for cartesian i.e. $r,\theta, z \rightarrow x, y, z$, see Figure 21, and second, the shape of the density function will be approximated by a function for which a solution to the wave equation is known.

Equation (5b) through (9b), (12), and (13) are assumed and the current, $\underset{\sim}{j}$, is taken to be rotation free ($\underset{\sim}{j} = - en_{eo}\underset{\sim}{v}_{e1}$).

$$\nabla \times \underset{\sim}{j} = 0 \tag{30}$$

For purely longitudinal waves the current is rotation free and therefore (30) represents the hypothesis stated above.

Combining the continuity equation (5b) and the divergence of the equation for electric field one obtains

$$\nabla \cdot \underset{\sim}{E} = - \frac{\nabla \cdot \underset{\sim}{j}}{\epsilon_o i\omega} \quad \text{or} \quad \underset{\sim}{E} = \frac{\underset{\sim}{j}}{i\omega\epsilon_o} .$$

This, of course, follows directly from Maxwell's equations with zero magnetic field.

The momentum equation, (6b), may then be written entirely in the variable $\underset{\sim}{j}$ yielding

$$0 = k^2 \underset{\sim}{j} + \nabla(\nabla \cdot \underset{\sim}{j}) - \frac{1}{3} \frac{\nabla n_{eo}}{n_{eo}} \nabla \cdot \underset{\sim}{j} \quad . \tag{31}$$

All functions are constant in the y direction as it corresponds to the θ coordinate - only the rotationally symmetric mode is being considered here. For the cutoff case, ($\frac{\partial}{\partial z} = 0$), the vector equation (31) reduces to a scalar equation.

A change of variable is now made[31].

$$j = \psi\, n_{eo}^{\frac{1}{6}} \tag{32}$$

This results in

$$0 = \frac{\partial^2 \psi}{\partial x^2} + \psi\left[k^2 - \frac{7}{36}\left(\frac{\partial n_{eo}}{\partial x}\frac{1}{n_{eo}}\right)^2 + \frac{1}{6}\frac{\partial^2 n_{eo}}{\partial x^2}\frac{1}{n_{eo}}\right] . \tag{33}$$

For sufficiently slowly changing n_{eo} functions, the last two terms in the brackets may be neglected, resulting in (34). (This matter is discussed in Appendix III).

$$0 = \frac{\partial^2 \psi}{\partial x^2} + k^2(x)\,\psi \tag{34}$$

A solution to the wave equation ,(34), for several special functions $k^2(x)$ is given by P. Epstein[32]. One of these functions, (35), represents a transition layer i.e. a smooth transition from $k^2(x) = k_o^2$ to $k^2(x) = -k_o^2$, see Figure 22.

$$k^2(x) = k_o^2\left(1 - \frac{2e^{mx}}{1+e^{mx}}\right) \tag{35}$$

The quantity k_o^2 in (35) is the value of $k^2(x)$ which exists far to the left of the transition region, namely in the region where the plasma waves may propagate but $\omega_p^2 \ll \omega^2$. Reference to equation (13) shows that $k_o^2 = \frac{\omega^2}{c_s^2}$. The wave is considered incident from this region of very tenuous plasma on the transition where it is reflected because k^2 is negative for positive values of x, that is, the core of the discharge.

Equations (34) and (35) can be solved through transformations which relate them to the hypergeometric differential equation, see reference 32. The solution (36) of these equations represents a standing wave (in $\underset{\sim}{j}$).

$$\psi = j\, n_{eo}^{-\frac{1}{6}} = m^{-\frac{1}{2}}\, \xi^{\frac{ik_o}{m}}\,(1-\xi)^{\frac{3}{2}}\, G \tag{36}$$

$$G = (-1)^{-\alpha} \frac{\Gamma(\alpha-\beta+1)\Gamma(1-\gamma)}{\Gamma(1-\beta)\Gamma(1+\alpha-\gamma)} F_1 + (-1)^{\gamma-1-\alpha} \frac{\Gamma(\alpha-\beta+1)\Gamma(\gamma-1)}{\Gamma(\gamma-\beta)\Gamma(\alpha)} F_2 \quad \text{for } x < 0$$

$$G = \xi^{-\alpha} F\left(\alpha, \alpha-\gamma+1, \alpha-\beta+1, \frac{1}{\xi}\right) \quad \text{for } x > 0$$

$$F_1 = F(\alpha, \beta, \gamma, \xi) \qquad F_2 = \xi^{1-\gamma} F(\alpha-\gamma+1, \beta-\gamma+1, 2-\gamma, \xi) \qquad \text{(36 con't)}$$

$$\alpha = 1 + \frac{k_o}{m}(1+i) \qquad \beta = 1 + \frac{k_o}{m}(-1+i) \qquad \gamma = 1 + i\,\frac{2K_o}{m}$$

$$\xi = -e^{mx}$$

F is the hypergeometric function and Γ is the gamma function.

The boundary condition is that j = 0 at r_w, the plasma-glass interface. That is, if a zero in the standing wave pattern, equation (36), coincides with the position of the wall, a resonance point has been found. For sufficiently negative values of x, for example in the region of the wall, the solution, (36), reduces to the sum of two exponential functions with imaginary arguments which may be associated with the incident and reflected waves. Also in this region one can obtain an expression for the phase of equation (36). In equation (37) V is the phase of the solution, (36), taken at the point x (x is negative).

$$V = \frac{\Gamma(\gamma-1)\Gamma(1-\beta)\Gamma(1+\alpha-\gamma)}{\Gamma(1-\gamma)\Gamma(\gamma-\beta)\Gamma(\alpha)} e^{-i2k_o x} \qquad (37)$$

The correct boundary condition is fulfilled when V, evaluated at the wall, has the value of π radians which corresponds to a reflection factor of - 1.

The calculation of the values of $(\omega^2/\overline{\omega_p^2})_{co}$ begins by determining the location of the x,y,z coordinate system, namely what value of radius, r_c, corresponds to x = 0 in the cartesian system. This matter is arbitrary, however, the method described is reasonable and will be followed. Since x = 0 is the point on the assumed profile curve, see Figure 22, where $k^2(x) = 0$ it is chosen to coincide with the radius at which $\omega^2 = \omega_p^2$, namely $k^2 = 0$, equation (13).

The basic steps in the calculation are:

1) For a given value of $\overline{\omega_p^2}$ a value of ω^2 is assumed. This determines r_c, that radius where $\omega^2 = \omega_p^2$. For all these calculations an electron density profile curve corresponding to large $r_w^2/\overline{\lambda_d^2}$ is used.
2) The origin of the x,y,z coordinate system is located at r_c.
3) $k_o^2 = \frac{\omega^2}{c_s^2}$ is computed.
4) The value of m, equation (35), is determined by requiring the $k^2(x) = k_o^2/2$ point on the assumed profile (35) to coincide with the $\omega_p^2 = \omega^2/2$ point. That is, the real electron density curve and the assumed density curve are made to correspond identically at two points, where $\omega^2 = \omega_p^2$ and where $\omega^2/2 = \omega_p^2$.
5) The value of the reflection factor V, referred to the wall, or $x = r_c - r_w$, is calculated by (37).

If the correct reflection factor, - 1, is not achieved another value of ω^2 is taken and steps 1 to 5 are repeated. The reflection factor of the function ψ is the same as that for j. The actual computation corresponding to steps 1 to 5, which is made using dimensionless quantities, can be completed for several ω values quickly by hand requiring only a table of gamma functions.

The great value of this approach lies in the fact that the $(\omega^2/\overline{\omega_p^2})_{co}$ values so calculated are quite independent of the parameter $r_w^2/\overline{\lambda_d^2}$ provided it is large enough. This is true because the shape of the profile function in the sheath region is the same for sufficiently large $r_w^2/\overline{\lambda_d^2}$ and a characteristic length, l_s, ("sheath thickness") is proportional to $(\overline{\lambda_d^2})^{1/2}$ which in turn is proportional to $(1/\overline{\omega_p^2})^{1/2}$. The length, l_w, associated with ω e.g. wavelength or inverse of propagation vector is proportional $1/\omega$. Significant for the propagation of the wave, that is, the solution of the eigenvalue problem, is the quantity l_s/l_w, which is proportional $(\overline{\lambda_d^2})^{1/2}\Big/\frac{1}{\omega}$ or $\omega/(\overline{\omega_p^2})^{1/2}$. Particular values of l_s/l_w (eigenvalues), corresponding to cutoff, yield the values $(\omega^2/\overline{\omega_p^2})_{co}$. As l_s/l_w is independent of $\overline{\lambda_d^2}$, so is $(\omega^2/\overline{\omega_p^2})_{co}$ also. The statement that the sheath thickness is proportional to $(\overline{\lambda_d^2})^{1/2}$ for sufficiently large values of $r_w^2/\overline{\lambda_d^2}$, or otherwise formulated, that the electron density distribution function in the sheath region, plotted in units of $(\overline{\lambda_d^2})^{1/2}$ approaches on asymptotic form,

is shown by the numerical calculations of Parker[17]. Also a particularly good discussion of this postulate (for the case of plane geometry) is given by Self[33]. This fact is born out by experiment. The results of this computation are shown in Figure 13.

The application of this calculation to the case of propagation will be discussed now. As the x coordinate corresponds to the radial measure in the discharge tube, the y to the azimuthal and z to axial, there is no variation in y of any function, and the derivatives in the z direction can be replaced with the propagation factor in the z direction, β. That is

$$\frac{\partial}{\partial z} \rightarrow i\beta \ .$$

The current $\underline{j}$ is assumed to have two components j_x and j_z. One obtains then for equation (31) in component form

$$0=(k^2-\beta^2)j_z + i\beta \frac{\partial j_x}{\partial x}$$

$$0=\frac{\partial^2 j_x}{\partial x^2} + k^2 j_x - \frac{1}{3}\frac{\partial n_{eo}}{\partial x}\frac{1}{n_{eo}}\left(\frac{\partial j_x}{\partial x} + i\beta j_z\right) + i\beta \frac{\partial j_z}{\partial x} \ . \qquad (37a,b)$$

From (37a) one obtains (38) which may be introduced into (37b) resulting in equation (39) which is an ordinary differential equation in the variable j_x.

$$j_z = -\frac{i\beta \frac{\partial j_x}{\partial x}}{k^2-\beta^2} \qquad (38)$$

$$0=\frac{\partial^2 j_x}{\partial x^2} + (k^2-\beta^2)j_x + \frac{\partial j_x}{\partial x}\left[\frac{-\beta^2}{k^2-\beta^2}\frac{1}{k^2}\frac{\partial k^2}{\partial x} - \frac{1}{3}\frac{1}{n_{eo}}\frac{\partial n_{eo}}{\partial x}\right] \qquad (39)$$

The singular term in (39) prevents one from utilizing a transformation such as equation (32). (A transformation such as (32) may be carried out but the additional terms which are introduced, see equation (33), are also singular.) The singular term indicates that the assymption of proportionality between

the electric field and the current is not permissable when the current is not parallel to the gradient in the electron density.

Because of the singular term in (39) calculations have been made only for $\beta = 0$, (equation (34)). These results are shown in Figure 13, the values of $(\omega^2/\overline{\omega_p^2})_{co}$ and in Figure 23, the function ψ vs radius. For bands occuring at higher values of $\omega^2/\overline{\omega_p^2}$, (than shown in Figure 13), the region of wave action then extends beyond the sheath region and, as the geometric approximations made here are no longer valid, the calculation was terminated.

Summary

In this work a coherent experimental and theoretical presentation of some modes of propagation along a plasma column are presented (high frequency, primarily electromagnetic, waves are not represented). Two of the propagation bands previously studied, namely the first in the n = 0 and n = 1 mode, are shown to be part of a series of propagation bands. The Tonks-Dattner resonances represent the cutoff conditions of the dipole mode. The higher bands of the rotationally symmetric mode observed here complete the presentation. To the author's knowledge the first report of experimental observations and theoretical calculations of propagation via the higher order bands is given in reference 28. During the preparation of this manuscript a further experimental report has been published[34]. The quadrapole resonances discussed by PNG[4] presumably also represent the cutoff points of propagation bands. Studies of the higher bands of the rotationally symmetric mode, which seem to be primarily electrostatic in nature, may provide experimental information on Landau damping etc. The correlation between the resonance points determined by h.f. probe measurements and the higher propagation bands indicates that a region of plasma much larger than that which immediately surrounds the probe is of importance.

Appendix I

When solving for the dispersion equation one must consider the field outside the plasma. This involves solution of the equation $\nabla^2\phi = 0$ in the glass discharge tube and in the surrounding air. These solutions to Laplace's equation must then be fitted together with proper boundary conditions at the glass-air interface and in turn with solutions for the plasma region at the plasma-glass interface.

In order that the dispersion equation may remain simpler in form it is convenient to represent the discharge tube and surrounding air as one homogeneous medium having an effective dielectric constant ε_E. The calculation of ε_E follows directly from the boundary conditions and will be shown for the rotationally symmetric mode.

Discharge tube: r_w = inside radius r_g = outside radius
ε_c = dielectric constant of the glass

Solution of $\nabla^2\phi = 0$ assuming $\phi = R(r)e^{i\beta z}$

In glass (index C) $r_w < r < r_g$ $R(r)_c = b_1 I_o(\beta r) + b_2 K_o(\beta r)$

In air (index D) $r_g < r$ $R(r)_D = b_3 K_o(\beta r)$

The equivalent solution (index E) $r_w < r$ $R(r)_E = b_4 K_o(\beta r)$

(The I_o function is singular for infinite argument).

The boundary conditions which follows from curl E finite and div E = 0 are:

At $r = r_w$; $\phi_c = \phi_E$ and $\varepsilon_c \frac{\partial \phi_c}{\partial r} = \varepsilon_E \frac{\partial \phi_E}{\partial r}$

$r = r_g$; $\phi_c = \phi_D$ and $\varepsilon_c \frac{\partial \phi_c}{\partial r} = \varepsilon_D \frac{\partial \phi_D}{\partial r}$

Choosing one of the b_n equal to unity the equations can be solved for $\varepsilon_E/\varepsilon_o$

$$\kappa^R = \frac{\varepsilon_E}{\varepsilon_o} = \frac{\varepsilon_c}{\varepsilon_o}\left\{1-\left(\frac{\varepsilon_c}{\varepsilon_o}-1\right)\frac{1+\frac{K_o(\beta r_w)}{K_1(\beta r_w)}\frac{I_1(\beta r_w)}{I_o(\beta r_w)}}{\left(1-\frac{K_o(\beta r_w)}{K_1(\beta r_g)}\frac{I_1(\beta r_g)}{I_o(\beta r_w)}\right)\frac{\varepsilon_c}{\varepsilon_o}+\left(\frac{K_o(\beta r_w)}{K_o(\beta r_g)}\frac{I_o(\beta r_g)}{I_o(\beta r_w)}-1\right)}\right\} \qquad (I.1)$$

A similar calculation may be made for the dipole mode resulting in

$$\kappa^D = \frac{\varepsilon_E}{\varepsilon_o} = \frac{\varepsilon_c}{\varepsilon_o}\left\{\frac{\left(\frac{\varepsilon_c}{\varepsilon_o}-1\right)\left(\frac{I_1'(\beta r_w)}{K_1'(\beta r_w)}-\frac{I_1(\beta r_w)}{K_1(\beta r_w)}\right)}{\left(\frac{I_1(\beta r_g)}{K_1(\beta r_g)}-\frac{I_1(\beta r_w)}{K_1(\beta r_w)}\right)-\frac{\varepsilon_c}{\varepsilon_o}\left(\frac{I_1'(\beta r_g)}{K_1'(\beta r_g)}-\frac{I_1(\beta r_w)}{K_1(\beta r_w)}\right)}\right\} \qquad (I.2)$$

with $$\frac{I_1'(\beta r_g)}{K_1'(\beta r_g)} = \frac{\beta r_g I_o(\beta r_g) - I_1(\beta r_g)}{-\beta r_g K_o(\beta r_g) - K_1(\beta r_g)} \,.$$

For $\frac{\varepsilon_c}{\varepsilon_o} = 4.3$ and $\frac{r_g}{r_w} = 1.19$ the following κ^R and κ^D values have been calculated.

βr_w	κ^D	κ^R
0.01	1.67	1.64
0.02	1.67	1.65
0.1	1.67	1.66
0.5	1.71	1.69
1.0	1.90	1.98
2.0	2.41	2.45
5.0	3.56	3.56
10.0	4.18	4.18
20.0	4.30	4.30

Appendix II

The boundary conditions which must be fulfilled at the point of discontinuity in the electron density may be determined either from equation (11) or from the initial equations, (5) through (9). In order to obtain these conditions from (11) the author found it necessary to replace the step function discontinuity in density by a ramp function and then, by use of a pertubation technique, to solve (11) in the ramp region. This calculations which is quite long and involved yields the required relations. Doctor P.E. Vandenplas of the École Royale Militaire, Bruxelles and Professor R.W. Gould of the California Institute of Technology pointed out that these boundary conditions may be obtained very simply from the initial equations ((5) through (9)). This method, which will be given here, has the additional advantage of allowing maximum physical insight in the calculation.

A formal simplification of the calculation is obtained if cartesian coordinates are used instead of cylindrical: $r \rightarrow x$, $\theta \rightarrow y$, $z \rightarrow z$. Therefore $\partial/\partial y = 0$ and $\partial/\partial z = i\beta$. Repeating the initial first order equations for convenience:

$$\frac{\partial \phi}{\partial x} = -E_{1x}$$

$$\frac{\partial E_{1x}}{\partial x} + \frac{\partial E_{1z}}{\partial z} = -\frac{e}{\varepsilon_0} n_1$$

$$\frac{\partial (n_0 v_x)}{\partial x} + \frac{\partial (n_0 v_z)}{\partial z} = -i\omega n_1$$

$$i\omega m_e n_0 v_x = -e n_0 E_{1x} + \frac{KT}{n_0}\frac{\partial n_0}{\partial x} n_1 - 3KT\frac{\partial n_1}{\partial x}$$

The physical quantities may now be ordered according to increasing "roughness" e.g. because of differentiation E_{1x} is "rougher" than ϕ etc.

In increasing roughness:

$$\left.\begin{matrix} \phi \rightarrow E_1 \rightarrow n_1 \\ n_0 v_1 \rightarrow n_1 \end{matrix}\right\} \rightarrow \frac{\partial n_1}{\partial x}$$

In case one of the variables is discontinuous across the step in electron density the $\partial n_1/\partial x$ function will exhibit the maximum "roughness". In the immediate vicinity of the step in n_o one may then neglect, in the momentum equation, the terms with E_{1x} and $n_o v_1$ compared with the $\partial n_1/\partial x$ term. This results in :

$$0 = \frac{KT}{n_o}\frac{\partial n_o}{\partial x} n_1 - 3KT\frac{\partial n_1}{\partial x}$$

One may integrate this equation from immediately before the step, $x = 0_-$, to a value of x immediately ofter the step, $x = 0_+$ (step located at $x = 0$):

$$\int_{x=0_-}^{x=0_+} \frac{1}{n_o}\frac{\partial n_o}{\partial x}\,dx = 3\int_{x=0_-}^{x=0_+} \frac{1}{n_1}\frac{\partial n_1}{\partial x}\,dx$$

n_o is a function only of x therefore $dx = \partial n_o/\partial x\; dx$. n_1 is a function of x and z (explicit time dependence of exp(iωt) assumed) therefore $dn_1 = \frac{\partial n_1}{\partial x}dx + \frac{\partial n_1}{\partial z}dz$.

The last term in the dn_1 expression contributes nothing to the integration and one obtains then

$$\ln(n_o(0_+)) - \ln(n_o(0_-)) = \ln(n_1^3(0_+)) - \ln(n_1^3(0_-)) \quad \text{or}$$

$$\frac{n_{1A}}{(\omega_{pA}^2)^{\frac{1}{3}}} = \frac{n_{1B}}{(\omega_{pB}^2)^{\frac{1}{3}}} .$$

The n_1 function exhibits a finite discontinuity and when one integrates the continuity equation and Poisson's equation similarly one obtains that the functions ϕ, E_{1x} and $n_o v_1$ (current) are continuous.

Appendix III

Part 1 :

Calculations will be made which show that the terms neglected in (34) are indeed negligible for the profile assumed and the values of the parameters e.g. m and k_o which exist at resonance. Equations (34), (35), and (13) are repeated here for convenience.

$$0 = \psi'' + \psi\left(k^2 - \frac{7}{36}\left(\frac{n_o'}{n_o}\right)^2 + \frac{1}{6}\frac{n_o''}{n_o}\right) \qquad n_o' \equiv \frac{\partial n_o}{\partial x} \text{ etc.} \tag{34}$$

$$k^2(x) = k_o^2\left(1 - \frac{2e^{mx}}{1+e^{mx}}\right) \tag{35}$$

$$k^2 = \frac{\omega^2 - \omega_p^2}{c_s^2} \tag{13}$$

Comparing (35) and (13), with $k_o = \omega^2/c_s^2$, one finds

$$\frac{\omega_p^2}{\omega^2} = \frac{2e^{mx}}{1+e^{mx}} \; . \tag{III.1}$$

With the relationship $\omega_p^2 = \frac{e^2 n_o}{\varepsilon_o m_e}$ one obtains

$$n_o = \omega^2 \frac{\varepsilon_o m_e}{e^2} \frac{2e^{mx}}{1+e^{mx}} \; . \tag{III.2}$$

It follows immediately that

$$\frac{n_o'}{n_o} = \frac{m}{1+e^{mx}} \qquad \text{and} \qquad \frac{n_o''}{n_o} = m^2 \frac{1-e^{mx}}{(1+e^{mx})^2} \; . \tag{III.2a,b}$$

Introducing (III.2a,b) into (34) and factoring k_o results in

$$0 = \psi'' + \psi k_o^2\left[\left(1 - \frac{2e^{mx}}{1+e^{mx}}\right) - \frac{m^2}{k_o^2}\left(\frac{1+6e^{mx}}{36(1+e^{mx})^2}\right)\right]$$

or $$0 = \psi'' + \psi k_o^2\left[A - \frac{m^2}{k_o^2} B\right] \; . \tag{III.3a,b}$$

The contention is that the bracketed term in (III.3b) is not significiently changed by the neglect of m^2/k_o^2 B. This is shown by calculating the terms A and B, and multiplying the latter with the values of m^2/k_o^2 which exist at the first and second resonances, i.e. the resonances for the two lowest values $(\omega^2/\overline{\omega_p^2})_{co}$. The parameter for the calculations is mx.

mx	A	B	1.90B	0.0256B
2	-0.75	0.018	0.034	0.00046
1	-0.46	0.035	0.066	0.00089
0.5	-0.24	0.043	0.080	0.0011
0	0.0	0.049	0.092	0.0012
-0.5	+0.24	0.050	0.095	0.0013
-1.0	+0.46	0.048	0.092	0.0012
-2.0	+0.75	0.040	0.075	0.0010

The value 1.90 corresponds to m^2/k_o^2 for the lowest resonance and 0.0256 to the next higher. Of course the neglected term, $m^2/k_o^2 B$, is not small compared to A at all values of mx as A goes through zero and B does not. However, for most values of mx the neglected term is less than 20 % of A for the lowest resonance. At the point of zero crossing of A consideration of the B term would only shift the zero crossing by a small amount. In the case of the second resonance the correction term is about 1 % as large as in previous case.

Part 2 :

The |Q| is evaluated for the analytical electron density profile assumed in Case C. The case of v_1 parallel to ∇n_o will be considered. Also v_1 will be taken to be

$$v_1 = v_M e^{i k(x) x} \qquad \text{with} \quad \frac{\partial v_1}{\partial x} = v_1 \left(ik + i x \frac{\partial k(x)}{\partial x} \right) .$$

The functions for k(x) and $n_o(x)$ are given by equations (35) and (III.2) respectively.

One obtains then the following as an expression for $Q = -\frac{3}{2}\left(1+\frac{n_o \nabla \cdot v_1}{v_1 \cdot \nabla n_o}\right)$:

$$Q = -\frac{3}{2}\left[1 + i\frac{k_o}{m}\left((1-e^{2mx})^{\frac{1}{2}} - \frac{mx e^{mx}}{(1-e^{2mx})^{\frac{1}{2}}}\right)\right] \; ; \; Q \equiv -\frac{3}{2}\left(1 + i\frac{k_o}{m} M\right)$$

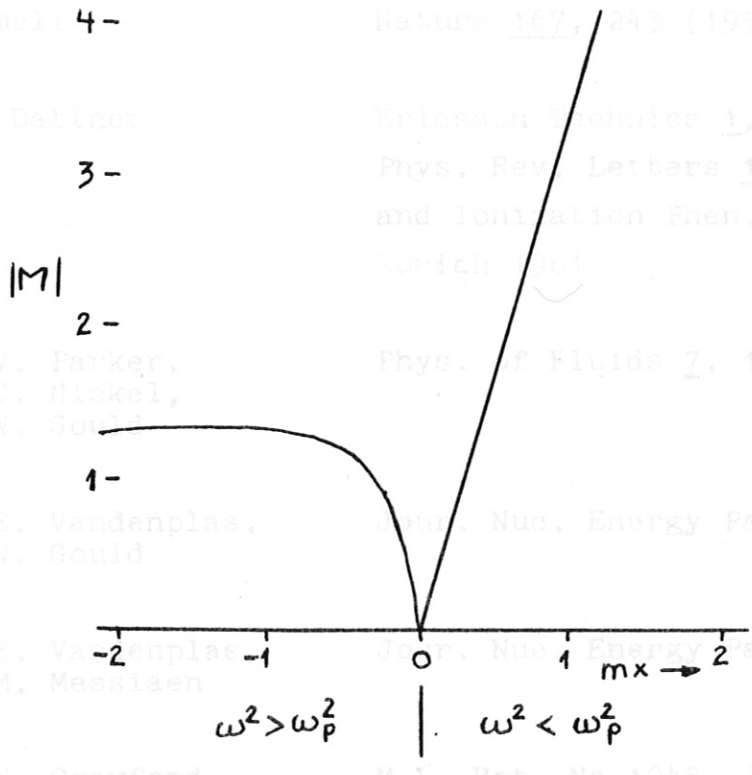

The values of k_o/m corresponding to the first two bands considered in Case C are 0.73 and 6.25. For this first band the $|Q|$ is about 2 in the propagating region whereas for the second band it is about 15. According to this estimate the $v_1 \cdot \nabla n_o$ term may be of importance for the band with $k_o/m = 0.73$. Since the very lowest band (not considered in Case C) is well described by the homogeneous plasma model it is expected that the neglect of the $v_1 \cdot \nabla n_o$ term in the pressure expression will cause little error.

References

1)	L. Tonks	Phys. Rev. 37, 1458, (1931) Phys. Rev. 38, 1219, (1931)
2)	Romell	Nature 167, 243 (1951)
3)	A. Dattner	Ericsson Technics 1, (1963) also Phys. Rev. Letters 10, 205, (1963) and Ionization Phen. in Gases, Munich 1961
4)	J.V. Parker, J.C. Nickel, R.W. Gould	Phys. of Fluids 7, 1489, (1964)
5)	P.E. Vandenplas, R.W. Gould	Jour. Nuc. Energy Part C 6, 449, (1964)
6)	P.E. Vandenplas, A.M. Messiaen	Jour. Nuc. Energy Part C 6, 459, (1964)
7)	F.W. Crawford	M.L. Rpt. No 1045, June 1963, Stanford University
8)	I. Langmuir, L. Tonks	Phys. Rev. 33,195, (1929)
9)	For example, Ginzburg	"The Propagation of Electromagnetic Waves in Plasma", §8, Pergamon Press
10)	For example, L. Spitzer	"Physics of Fully Ionized Gases", Intersc. Publishers
11)	D. Bohm, E.P. Gross	Phys. Rev. 75, 12, 185 (1949)
12)	H.M. Mott-Smith, I. Langmuir	Phys. Rev. 28, 727 (1926)
13)	B. Agdur, B. Enarder	Jour. Appl. Phys. 33, 2, (1962)

14) B. O'Brien — European Study Group on Fusion, Stockholm, April 1963

15) S.B. Cohn, N.P. Weinhouse — Microwave Journal 7, 2, (1964)

16) For example, S.Ramo, J.R. Whinnery — "Fields and Waves in Modern Radio", Chapt. 8 John Wiley and Sons

17) J.V. Parker — Phys. Fluids 6, 1657, (1963) also C.I.T. Report No 19 Contract Nonr 220 (13), December 1962

18) A.M. Messiaen P.E. Vandenplas — Phys. Letters 2, 4, 193 (1962)

19) P.E. Vandenplas, A.M. Messiaen — Nuc. Fission 5, 47, (1965)

20) A.M. Messiaen, P.E. Vandenplas — Nuc. Fission 5, 56, (1965)

21) A.M. Messiaen P.E. Vandenplas — Physica 30, 2309 (1964)

22) W.O. Schumann — Zeitschr. f. Angew. Phys. 17, 442, (1960)

23) W.C. Hahn — General Electric Rev. 42, 258, (1939)

24) S. Ramo — Phys. Rev. 36, 276, (1939)

25) A.W. Trivelpiece, R.W. Gould — Jour. Appl. Phys. 30, 11, (1959)

26) A. Schlüter — Zeitschr. f. Naturforschg. 5a, 73, (1950)

27) J.D. Jackson — Jour. Nucl. Energy Part C, 1, 178 (1959/60)

28) B. O'Brien, R.W. Gould, J.V. Parker — Phys. Rev. Letters 14, 630, (1965)

29) P. Weissglas — Jour. Nuc. Energy Part C 6, 251, (1964)

30) R.W. Gould — Proceedings of the Lindy Conference on Plasma Oscillations, 1959

31) For example, Margenau, Murphy — "Mathematics of Physics and Chemistry I", § 2.10, Van Nostrand

32) P. Epstein — Proc. Nat. Acad. Science 16, 10, (1930) also Brekhovskikh "Waves in Layered Media", Chapt.III, Academic Press

33) S.A. Self — Phys. of Fluids 6, 1762, (1963)

34) B. Keržar, P. Weissglas — Electronics Letters 1, 43, (1965)

Figure Captions

1. Discharge apparatus.

2. Electron temperature, T_e, as function of discharge current, $f(I_A)$, at 26°C mercury temperature. Electron temperature vs temperature of coldest point in discharge apparatus, $f(T_{Hg})$. Neutral gas pressure, data from "Handbook of Chemistry and Physics".

3. Couplers used to excite and receive waves: (a) coaxial re-entrant cavity, n = 0 mode; (b) single ring device, n=0 mode; (c) dipole device, n = 1 mode; (d) hf. probe connection.

4. Superheterodyne receiver, top. Phase sensitive receiver, bottom. (The plasma is schematically represented between two horns)

5. (a) Signal transmitted between two n = 0 couplers (Figure 3a) as received by superheterodyne receiver (N.B. the logarithmic scale). Frequency constant, 1000 Mcps, discharge current i.e. plasma density varied. The strong transmission band at 0.4 amperes discharge current is due to spurious coupling to the dipole mode (compare Figure 7).
(b) ω-β diagram for the n = 0 mode for propagation in anode to cathode, A → K, direction and cathode to anode, K → A, direction . Weak signals and interference reduce the accuracy of measurements of higher order bands and measurement in the region of $\beta \sim 0$.

6. Cut off values of n = 0 and n = 1 modes versus $r_w^2/\overline{\lambda}_d^2$ and resonance points for h.f. probe.

7. (a) Signal transmitted between two n = 1 couplers (Figure 3c) as received by superheterodyne receiver. Frequency constant, 1000 Mcps, discharge current i.e. plasma density varied. The transmission band present at values of $\omega^2/\overline{\omega_p^2}$ smaller than 0.15 is due to spurious coupling to the lowest n = 0 band

(compare Figure 5a). The jagged pattern on the lowest dipole band, ($\omega^2/\overline{\omega_p^2} \sim 0.2$), is due presumably to interference between the strong backward wave and the weaker forward wave region of propagation (see 7b).
(b) ω-β diagram for lowest dipole band; A → K propagation direction from anode to cathode, K → A from cathode to anode. Due to interference with the n = 0 mode no ω-β measurements could be made for the higher bands.

8. Experimental arrangement for observing dipole cutoff points.

9. Top two curves show power transmitted through wave guide (see Figure 8). The recorder sensitivity differed by a factor of two. The lower two curves show the voltage of receiver connected to a n = 0 coupler mounted on the discharge tube - the base lines have been shifted for clarity (recorder sensitivity for the lower two curves is the same).

10. Power transmitted through the cavity as a function of discharge current for many discrete frequencies. For clarity one curve, measured at 1070 Mcps, has been singled out. The coupling to the cavity is shown schematically.

11. (a) Block diagram for hf. probe measurements.
(b) Probe voltage versus discharge current for a constant frequency of 1000 Mcps.

12. Electron density profiles for a mercury positive column. Courtesy of J. Parker[17].

13. Experimental and theoretical curves of $(\omega^2/\overline{\omega_p^2})_{co}$ vs $r_w^2/\overline{\lambda_d^2}$ for the n = 0 mode. The theoretical curves are for the Cases A, B, and C. As Case C is applicable only for large values of $r_w^2/\overline{\lambda_d^2}$ it is represented by horizontal lines signifying an asymptotic value of $(\omega^2/\overline{\omega_p^2})_{co}$. The values of $\omega^2/\overline{\omega_p^2}$ for which $k_a = k_b = 0$ are shown. These parameters are of significance for Case B. One observes that at values of $\omega^2/\overline{\omega_p^2}$ larger than those for $k_a = 0$ a situation exists similar to that present in Case A. That is, the spacing of the curves becomes very

small (at large values of $r_w^2/\overline{\lambda_d^2}$). At the values of $\omega^2/\overline{\omega_p^2}$ larger than those for $k_a = 0$ the solutions of the wave equation in the entire plasma are of an oscillating nature. For Case A this condition exists at values of $\omega^2/\overline{\omega_p^2}$ larger than 1.

14. Theoretical (Case A and B) and experimental ω-β curves for $r_w^2/\overline{\lambda_d^2} = 240$ - corresponding to 10 ma discharge current and Hg vapor pressure determined by 26°C waterbath. Measurement of higher bands was precluded because of interference with the n = 1 mode. The small circles show the values of $\omega^2/\overline{\omega_p^2}$ which correspond to $k_a = k_b = 0$ - refer to Case B. The slope of the line at the bottom represents the velocity $(3KT/m)^{1/2}$.

15. Theoretical (Case A and B) and experimental ω-β curves for $r_w^2/\overline{\lambda_d^2} = 3500$-corresponding to 100 ma and 26° C. See caption Figure 14 for further explanation.

16. Theoretical (Case A) and experimental ω-β curves for $r_w^2/\overline{\lambda_d^2}$ = 40000-corresponding to 1000 ma and 26°C. Calculations for Case B could not be carried out as the arguments of the I-functions would be of the order of 100, corresponding to a value of the function too large for the computer.

17. Experimental and theoretical (Case A)$(\omega^2/\overline{\omega_p^2})_{co}$ vs $r_w^2/\overline{\lambda_d^2}$ curves for n = 1 mode.

18. Theoretical (Case A) and experimental ω-β curves for $r_w^2/\overline{\lambda_d^2}$ = 240-corresponding to 10 ma, discharge current and Hg vapor pressure determined by 26°C waterbath. B indicates observed backward waves. Measurements of higher bands is difficult because of low signal levels and interference with the n = 0 mode. Signal level is also low at large values of βr_w. The slope of the line at the bottom represents the velocity $(3\ KT/m)^{1/2}$.

19. Theoretical (Case A) and experimental ω-β curves for $r_w^2/\overline{\lambda_d^2}$ = 3500-corresponding to 1000 ma and 26°C (see caption Fifure 18). Measurement of the third and higher bands was pre-

vented by poor signal levels.

20. Theoretical (Case A) and experimental ω-β curves for $r_w^2/\overline{\lambda_d^2}$ = 40000-corresponding to 1000 ma and 26°C (see caption Figure 18). Higher bands, occurring at frequencies above 1600 Mcps, could not be measured because of resonances in the microwave dipole circuitry.

21. Relationship between cylindrical and cartesian coordinate systems (Case C).

22. Curve of assumed analytical $k^2(x)$ function (Case C).

23. ψ vs x for the second "longitudinal" transmission band, $(\omega^2/\overline{\omega_p^2})_{co}$ = 0.7, considered in Case C. Relative units for ψ. The position x = 0 corresponds to r - r_c - here r_c = 0.885 r_w. The value of $r_w^2/\overline{\lambda_d^2}$ is $0.43 \cdot 10^5$. The position of the wall, namely the value of x corresponding to r = r_w, is - 1.56. The curve to the left of this point is purely a mathematical plot of ψ and does not represent the physical phenomena.

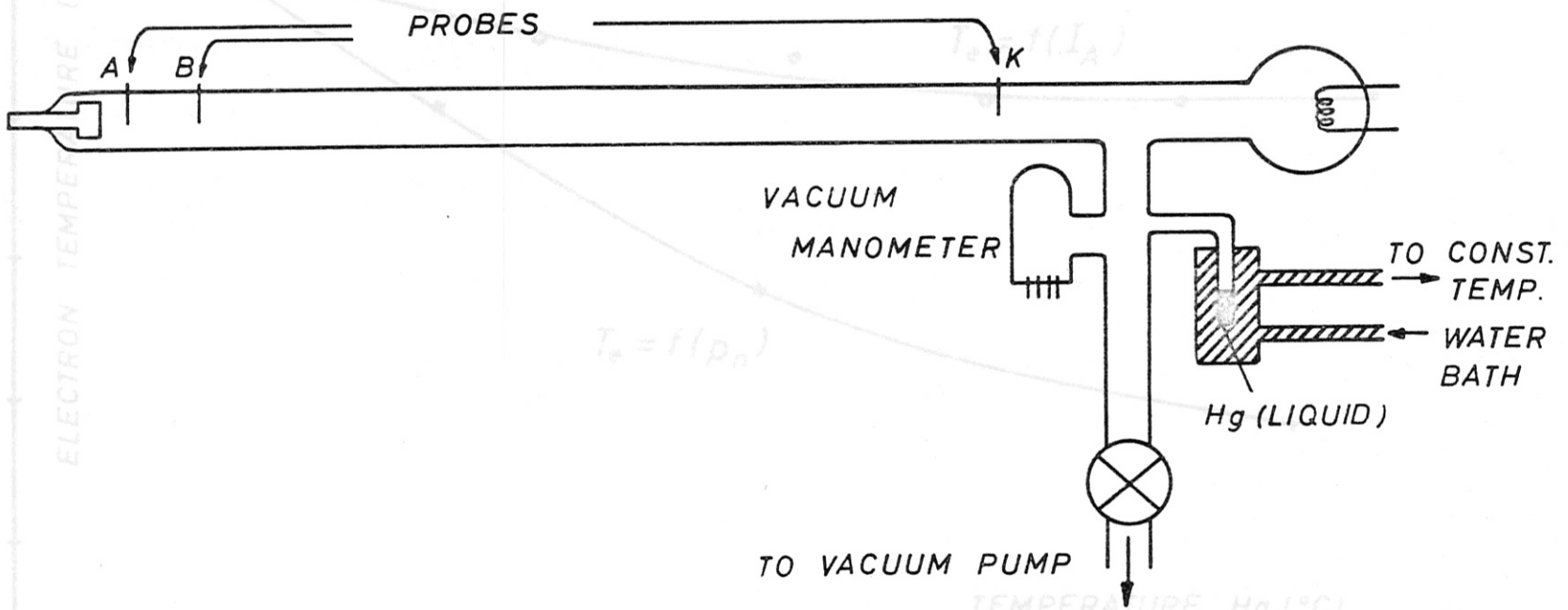
PROBES
A
B
K
VACUUM
MANOMETER
TO CONST.
TEMP.
WATER
BATH
Hg (LIQUID)
TO VACUUM PUMP

FIG. 1

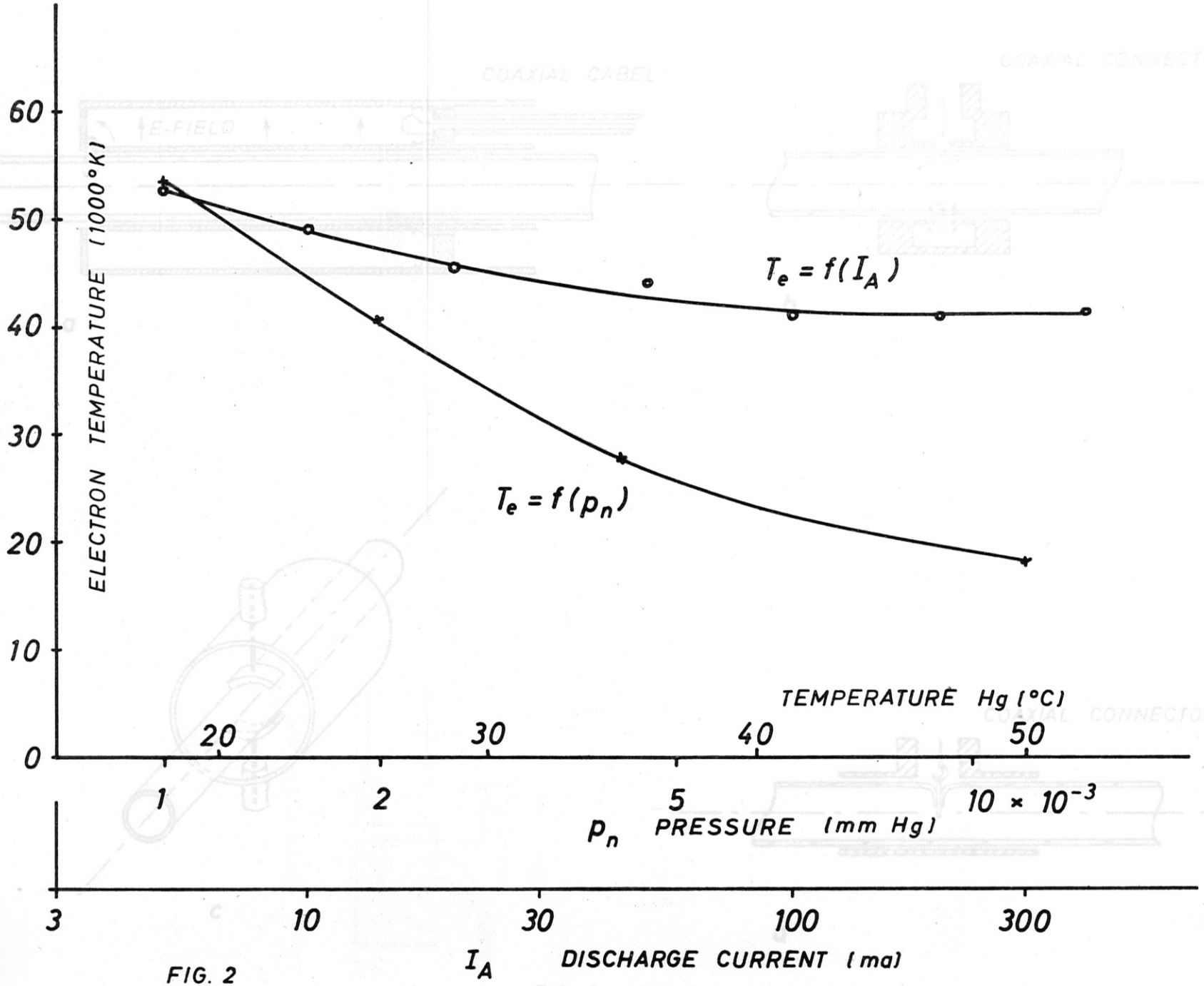
60
50
40
30
20
10
0
ELECTRON TEMPERATURE (1000°K)
$T_e = f(I_A)$
$T_e = f(p_n)$
TEMPERATURE Hg (°C)
20
30
40
50
1
2
5
10 × 10⁻³
p_n PRESSURE (mm Hg)
3
10
30
100
300
I_A DISCHARGE CURRENT (ma)

FIG. 2

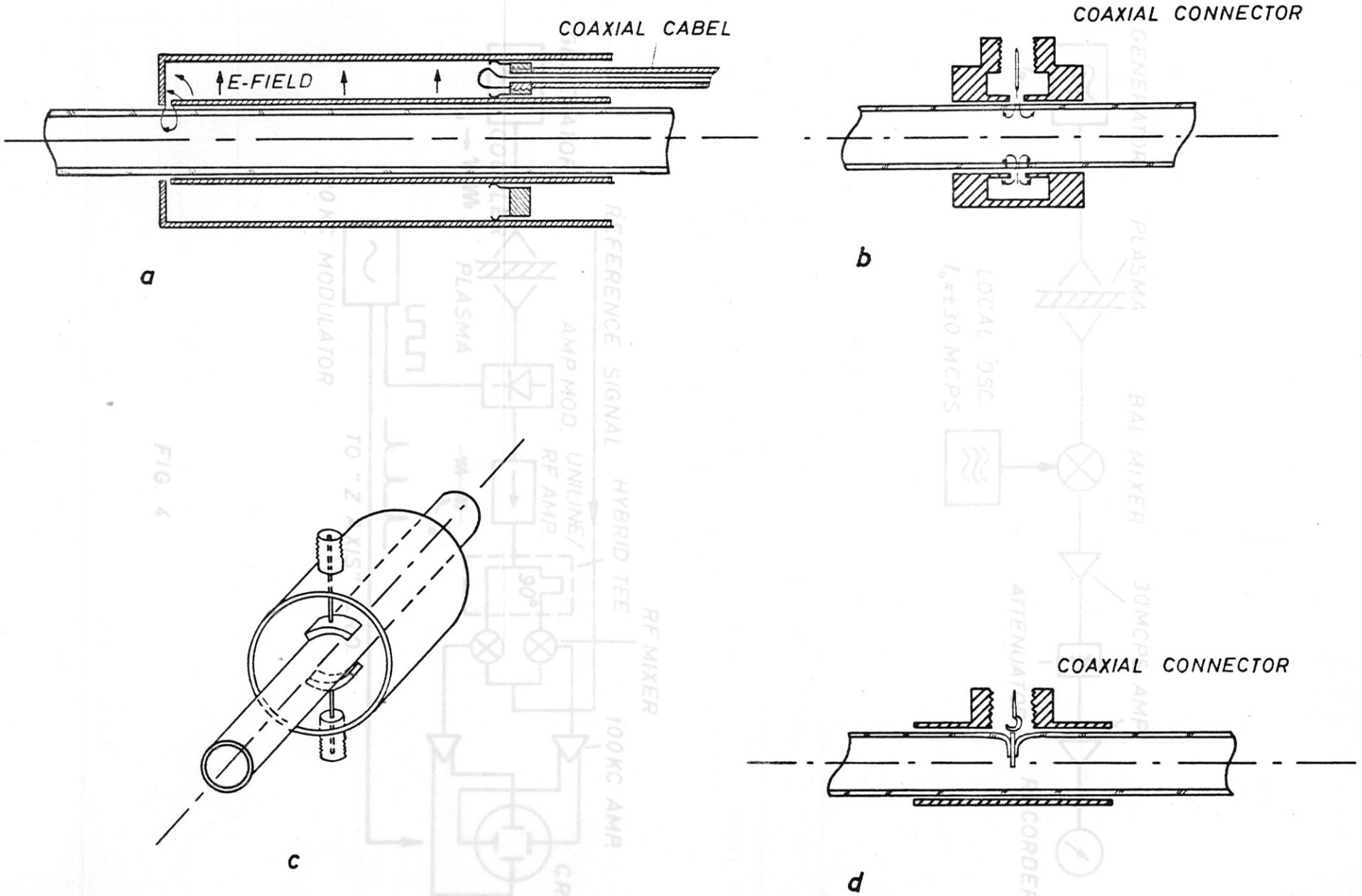
COAXIAL CABEL
E-FIELD
a
COAXIAL CONNECTOR
b
c
COAXIAL CONNECTOR
d

FIG. 3

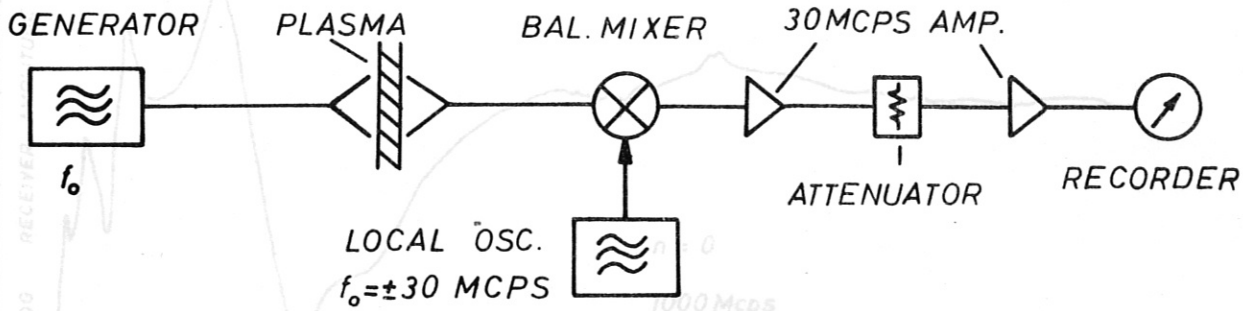
GENERATOR
PLASMA
BAL. MIXER
30MCPS AMP.
f_o
ATTENUATOR
RECORDER
LOCAL OSC.
$f_o = \pm 30$ MCPS

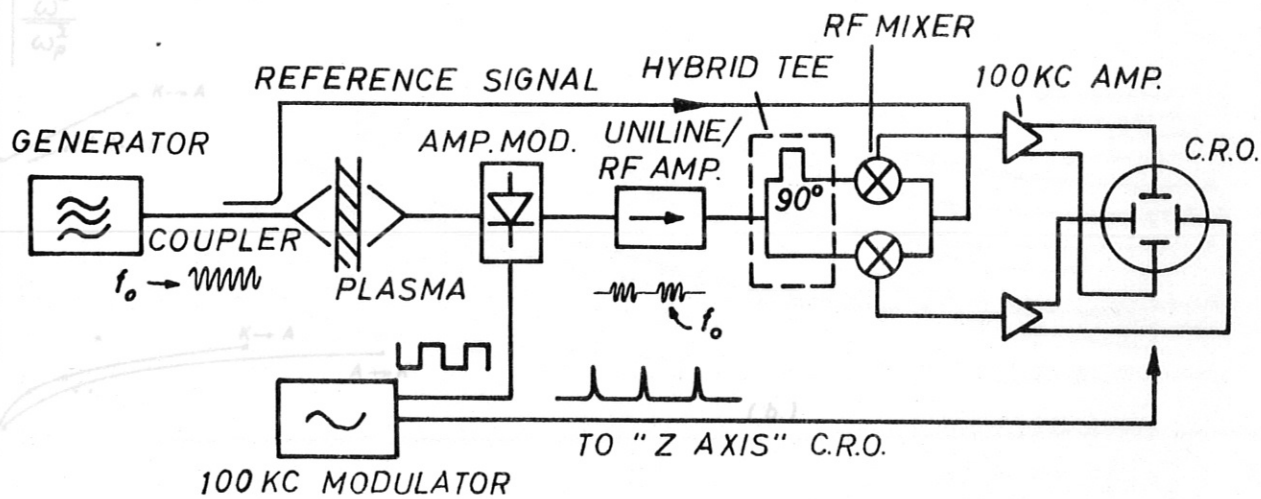
RF MIXER
REFERENCE SIGNAL
HYBRID TEE
100KC AMP.
GENERATOR
AMP. MOD.
UNILINE/
RF AMP.
C.R.O.
90°
COUPLER
f_o
PLASMA
f_o
TO "Z AXIS" C.R.O.
100 KC MODULATOR

FIG. 4

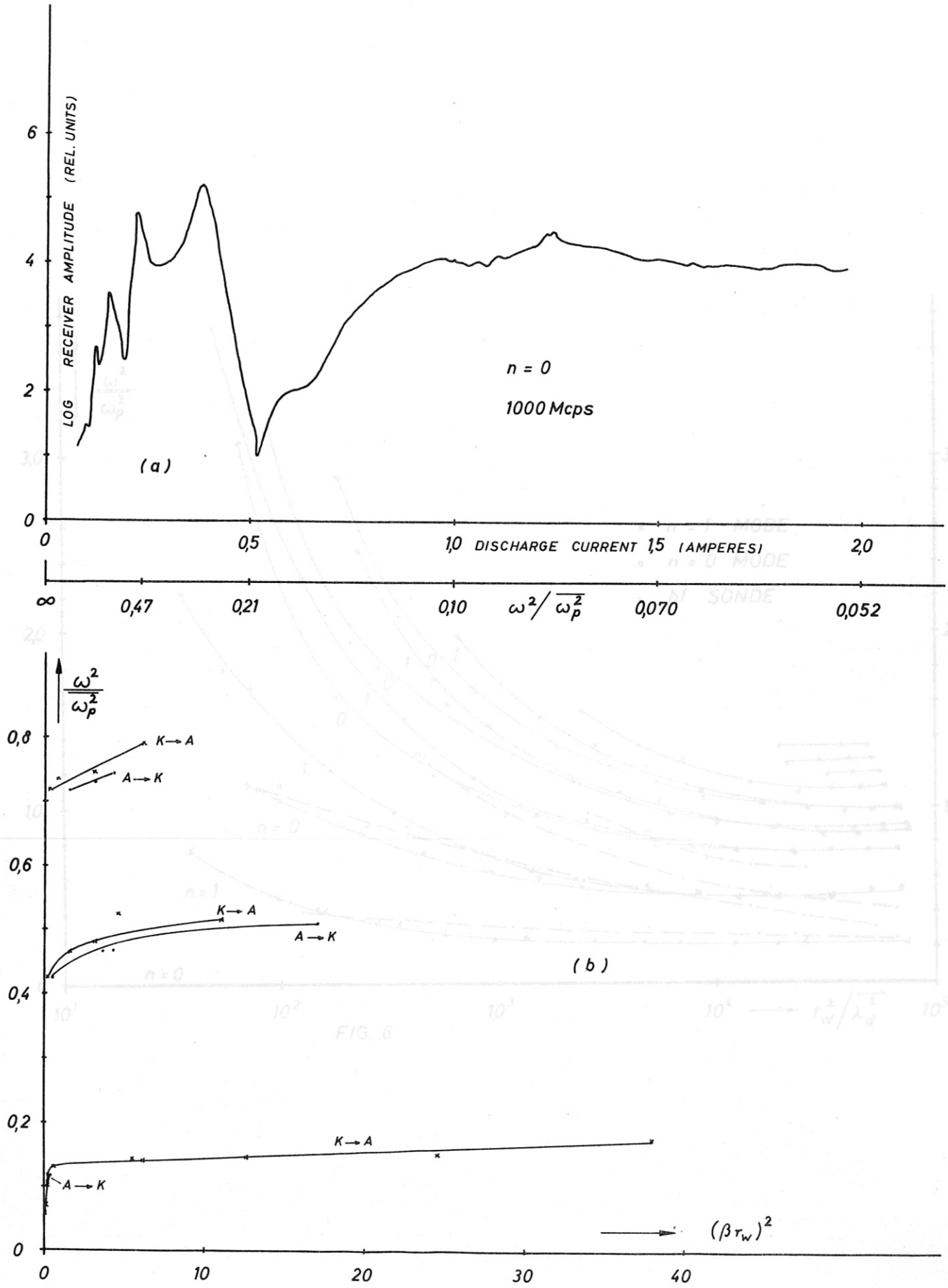
LOG RECEIVER AMPLITUDE (REL. UNITS)
6
4
2
0
n = 0
1000 Mcps
(a)
0
0,5
1,0
DISCHARGE CURRENT 1,5 (AMPERES)
2,0
∞
0,47
0,21
0,10
ω²/ω̄ₚ²
0,070
0,052
ω²/ωₚ²
0,8
0,6
0,4
0,2
0
K→A
A→K
K→A
A→K
(b)
K→A
A→K
(βr_w)²
0
10
20
30
40

FIG. 5

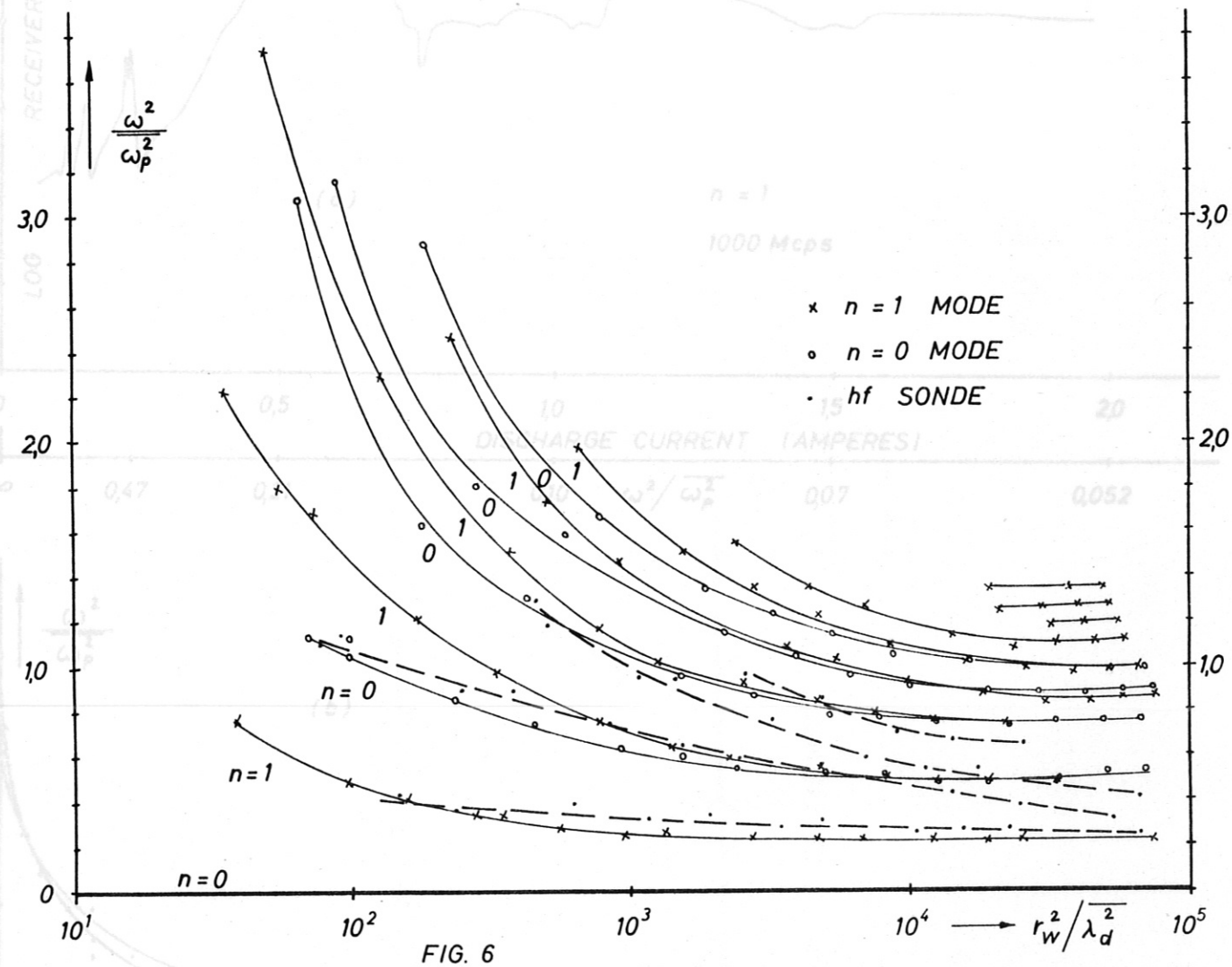
$\frac{\omega^2}{\omega_p^2}$
3,0
2,0
1,0
0
10^1
10^2
10^3
10^4
10^5
$r_w^2/\overline{\lambda_d^2}$
× n = 1 MODE
∘ n = 0 MODE
· hf SONDE
n = 0
n = 1
n = 0
1
0

FIG. 6

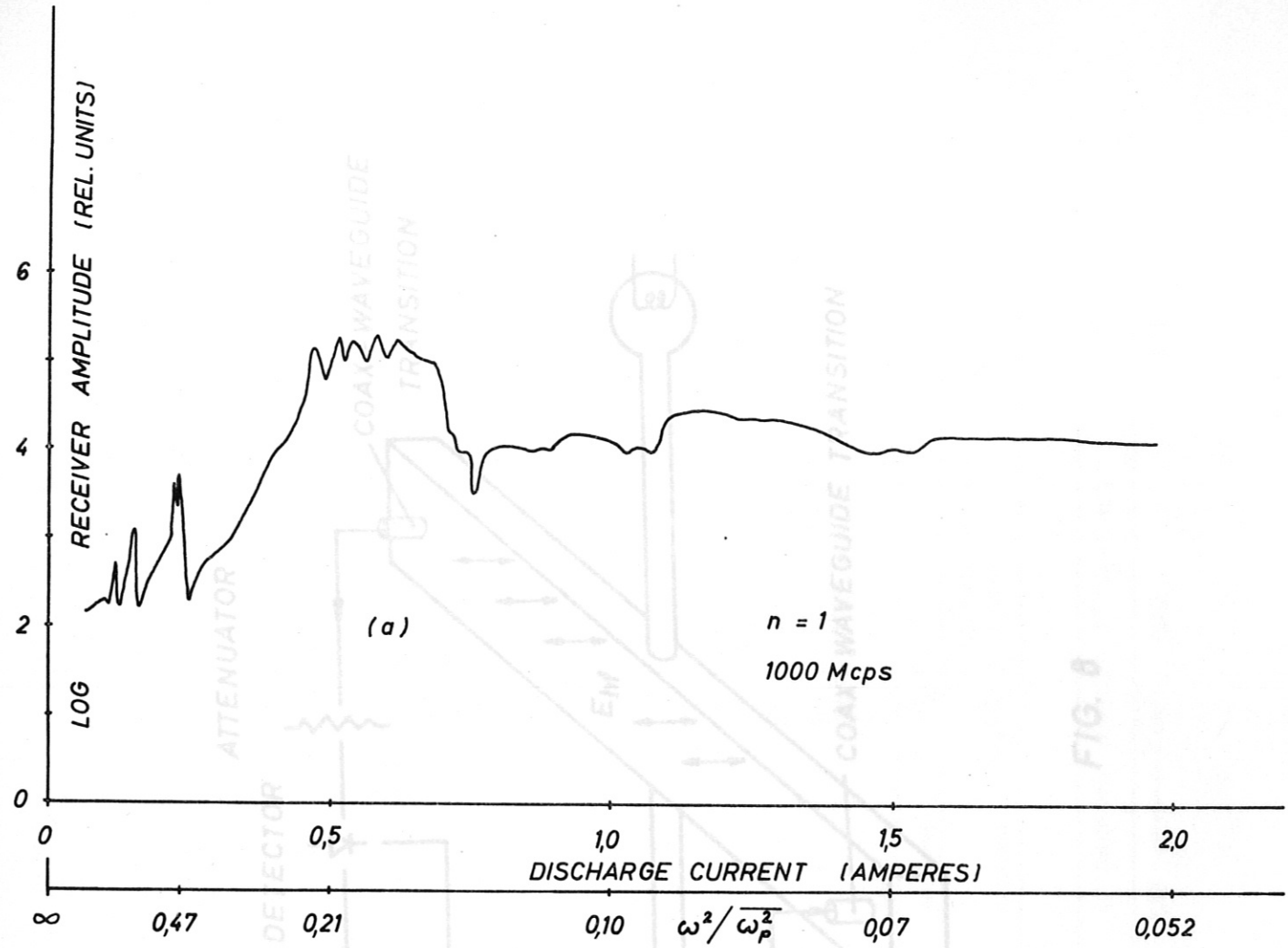
RECEIVER AMPLITUDE (REL. UNITS)
LOG
6
4
2
0
(a)
n = 1
1000 Mcps
0
0,5
1,0
1,5
2,0
DISCHARGE CURRENT (AMPERES)
∞
0,47
0,21
0,10
ω²/ω̄ₚ²
0,07
0,052

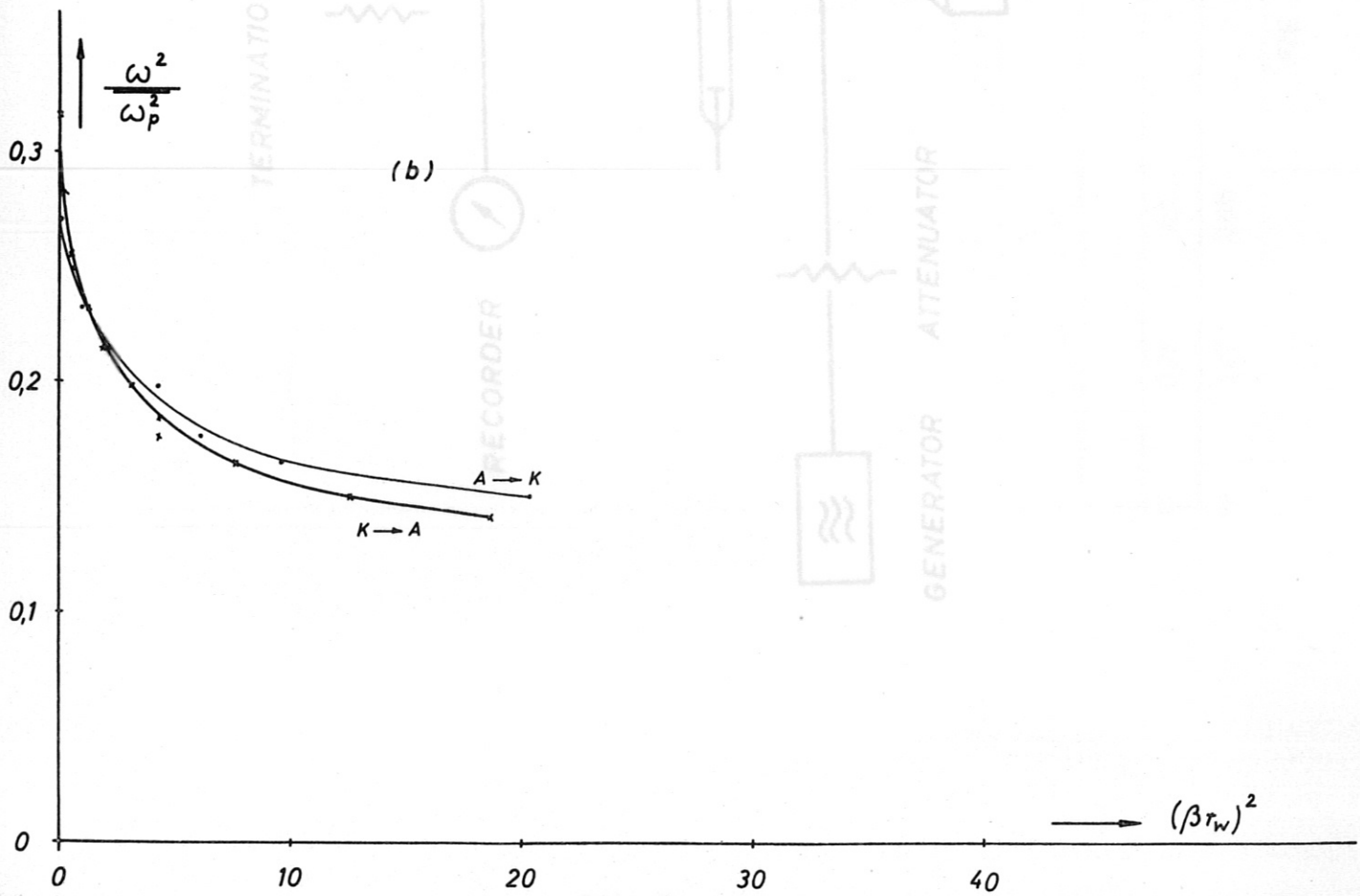
ω²/ωₚ²
(b)
0,3
0,2
0,1
0
A → K
K → A
0
10
20
30
40
(βrw)²

FIG. 7

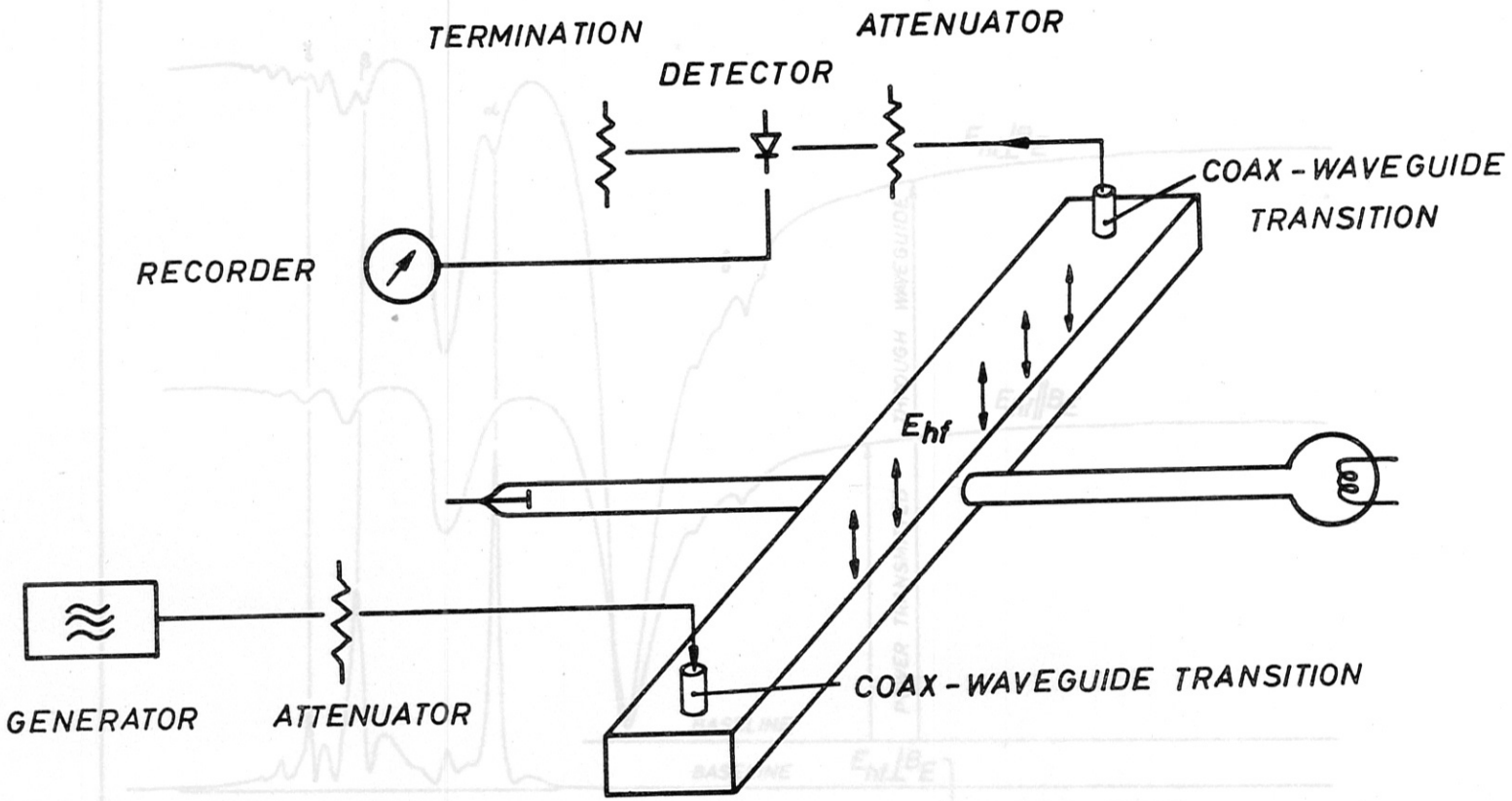
TERMINATION
DETECTOR
ATTENUATOR
COAX - WAVEGUIDE
TRANSITION
RECORDER
E_{hf}
GENERATOR
ATTENUATOR
COAX - WAVEGUIDE TRANSITION

FIG. 8

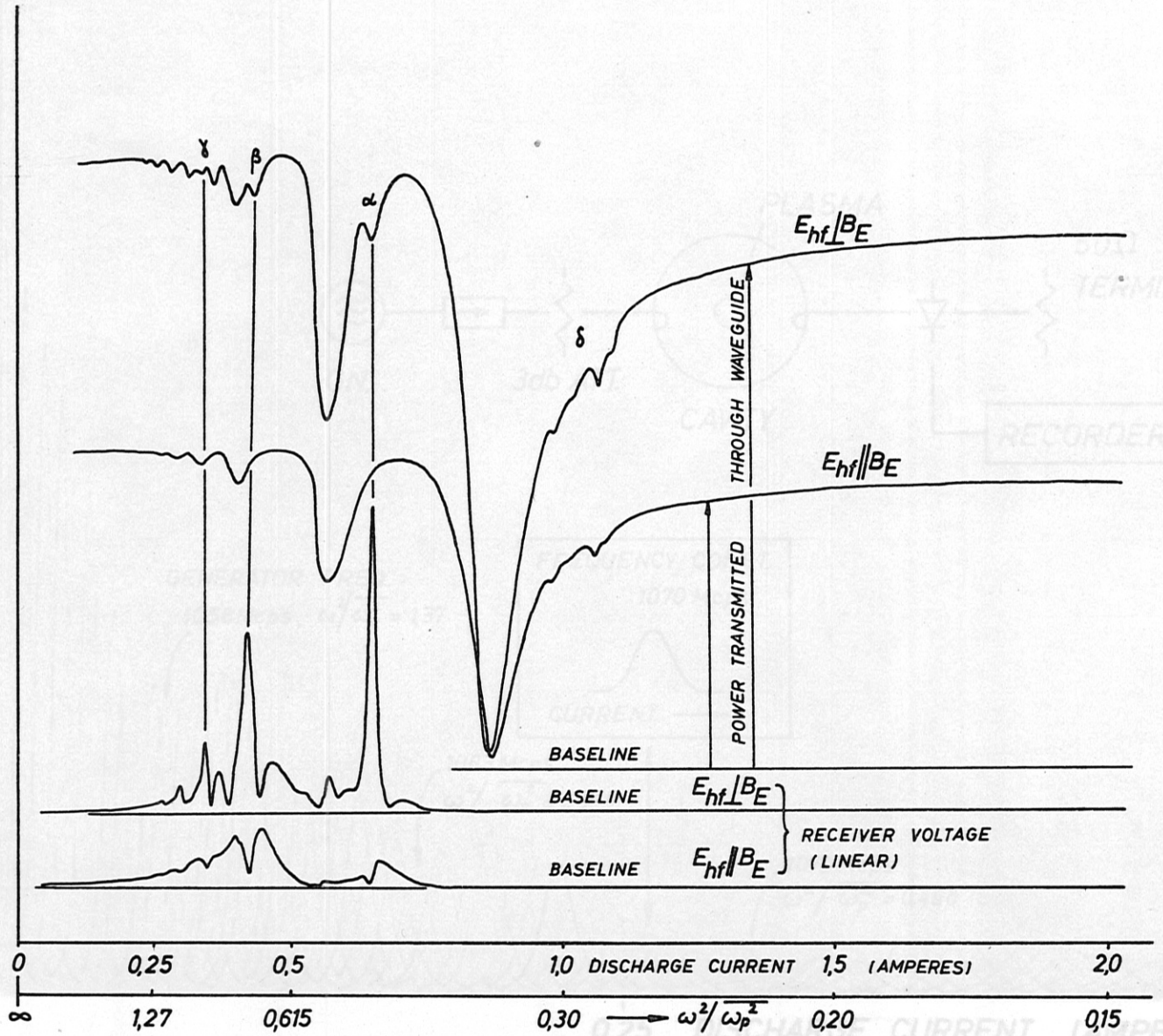
γ
β
α
δ
$E_{hf}\perp B_E$
$E_{hf}\parallel B_E$
THROUGH WAVEGUIDE
POWER TRANSMITTED
BASELINE
BASELINE
$E_{hf}\perp B_E$
BASELINE
$E_{hf}\parallel B_E$
RECEIVER VOLTAGE (LINEAR)
0
0,25
0,5
1,0 DISCHARGE CURRENT
1,5 (AMPERES)
2,0
∞
1,27
0,615
0,30 → $\omega^2/\overline{\omega_p^2}$
0,20
0,15

FIG. 9

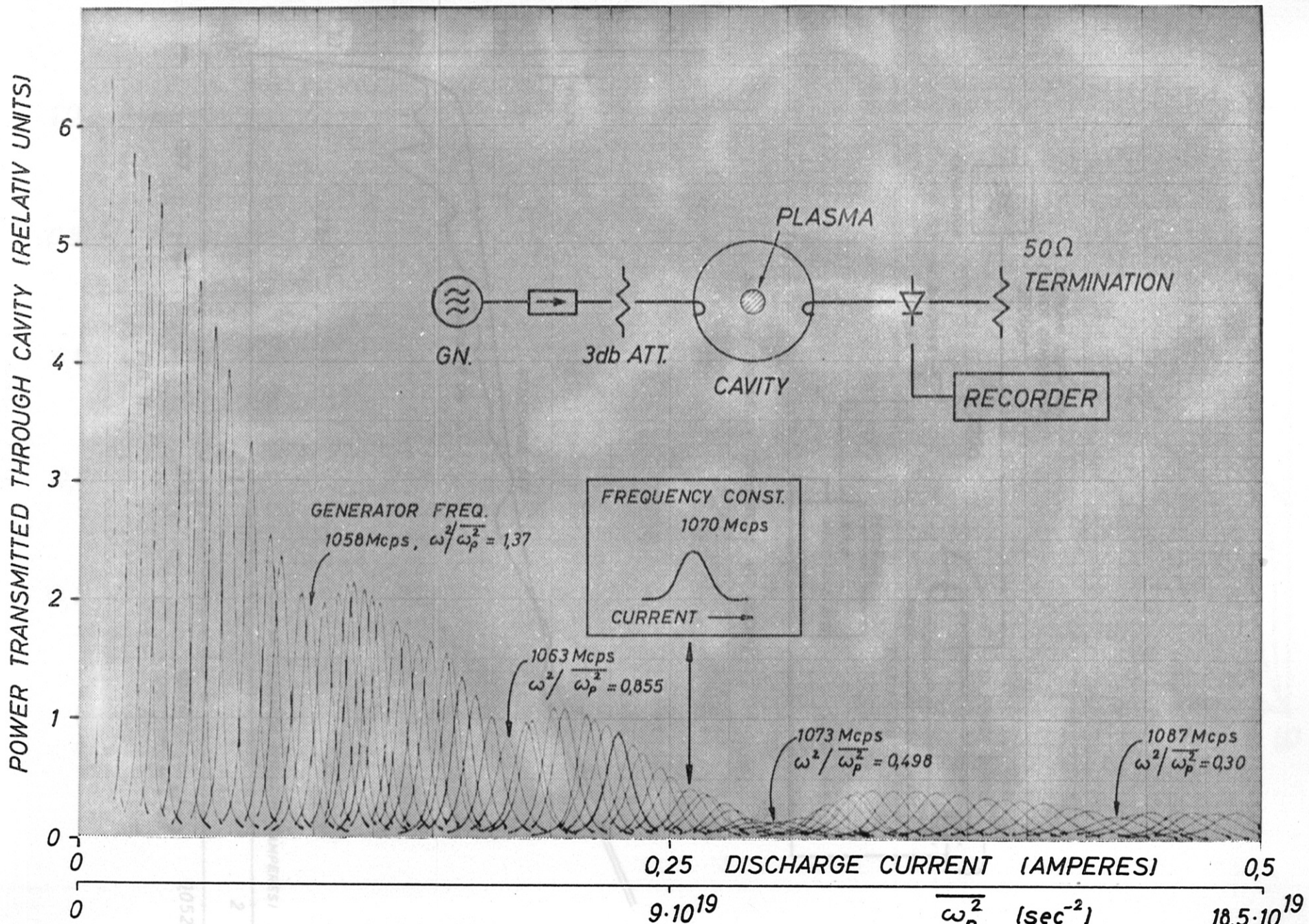
POWER TRANSMITTED THROUGH CAVITY (RELATIV UNITS)
6
5
4
3
2
1
0
PLASMA
50Ω TERMINATION
GN.
3db ATT.
CAVITY
RECORDER
FREQUENCY CONST.
1070 Mcps
CURRENT
GENERATOR FREQ.
1058Mcps, $\omega^2/\overline{\omega_p^2} = 1{,}37$
1063 Mcps
$\omega^2/\overline{\omega_p^2} = 0{,}855$
1073 Mcps
$\omega^2/\overline{\omega_p^2} = 0{,}498$
1087 Mcps
$\omega^2/\overline{\omega_p^2} = 0{,}30$
0
0,25
DISCHARGE CURRENT (AMPERES)
0,5
0
$9 \cdot 10^{19}$
$\overline{\omega_p^2}$ (sec^{-2})
$18{,}5 \cdot 10^{19}$

FIG. 10

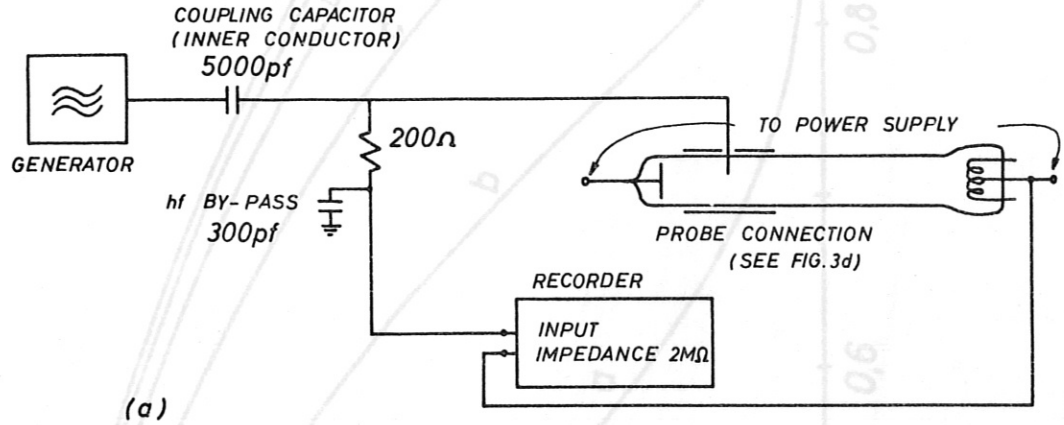

(a)

ALL HIGH FREQUENCY CONNECTIONS ARE COAXIAL

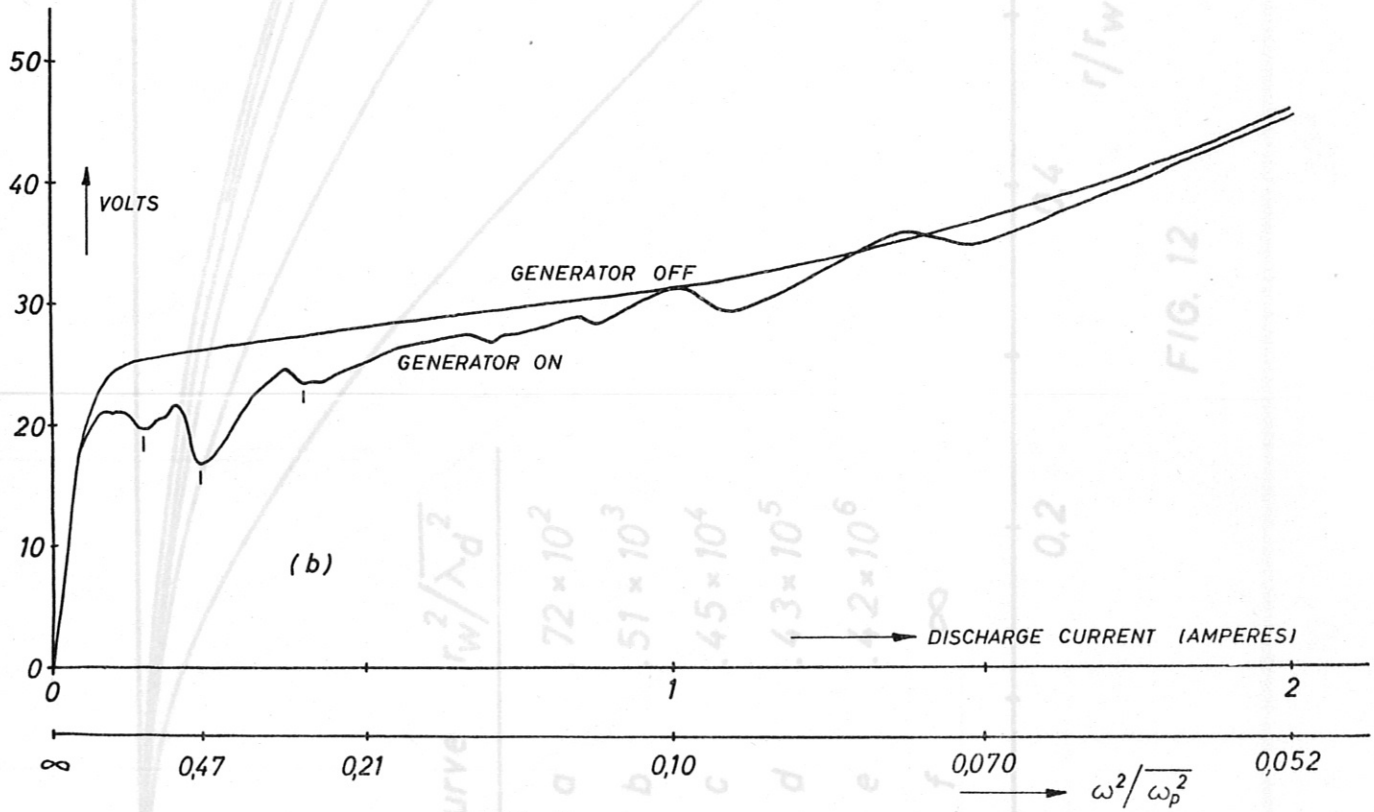

FIG. 11

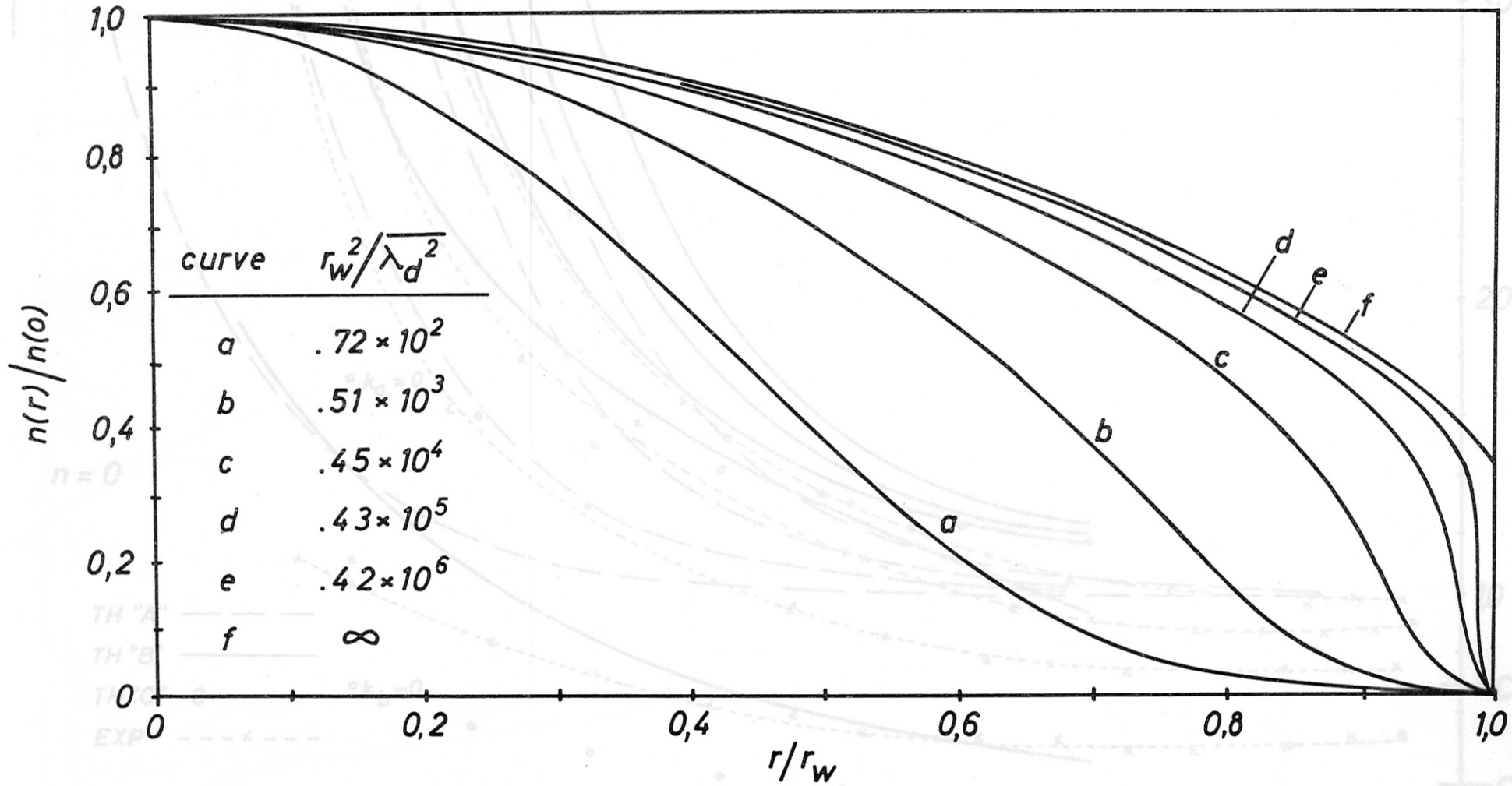
1,0
0,8
0,6
0,4
0,2
0
0
0,2
0,4
0,6
0,8
1,0
n(r)/n(o)
r/r_w
curve
r_w²/λ_d²
a
.72 × 10²
b
.51 × 10³
c
.45 × 10⁴
d
.43 × 10⁵
e
.42 × 10⁶
f
∞
a
b
c
d
e
f

FIG. 12

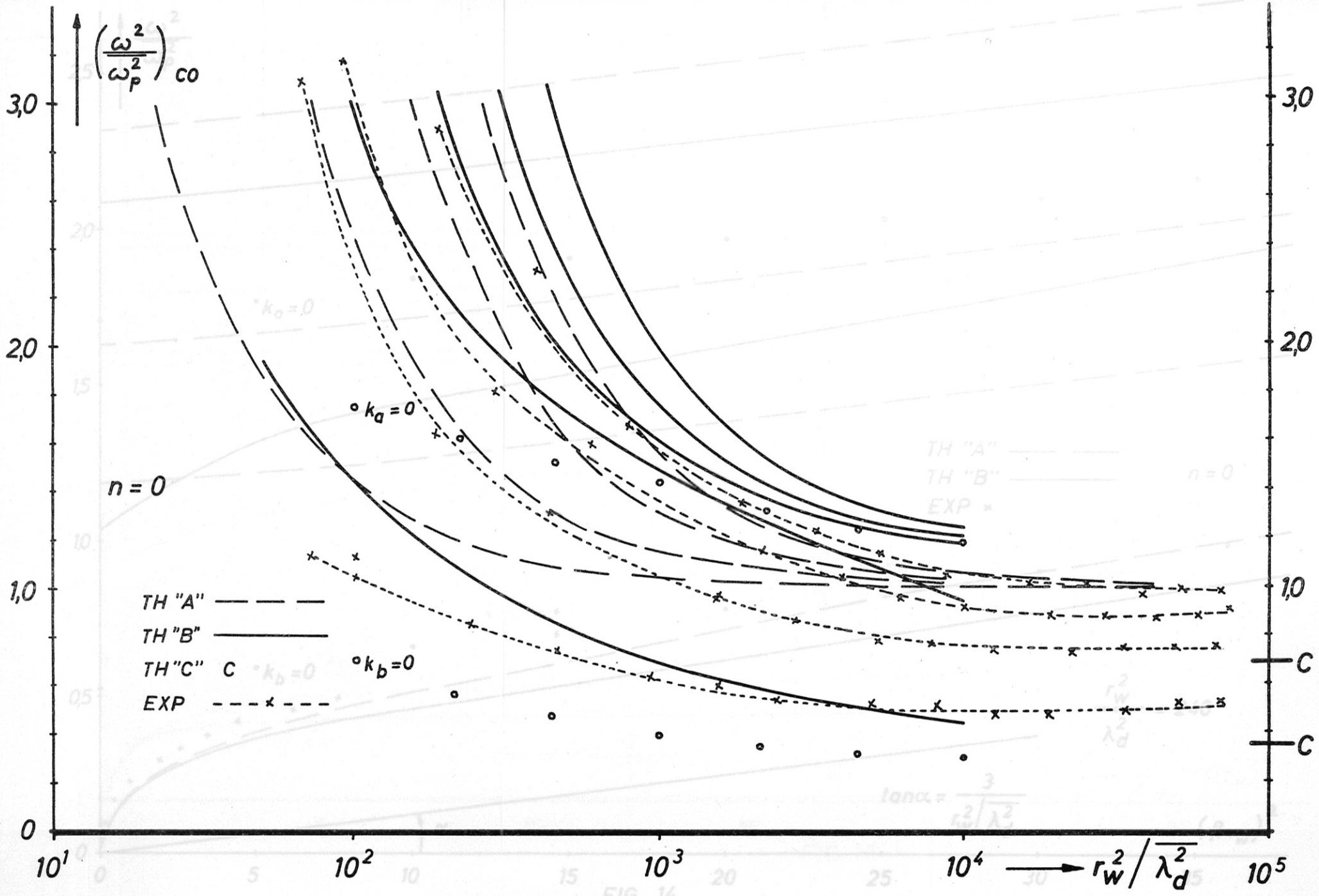
$\left(\frac{\omega^2}{\omega_p^2}\right)_{CO}$
3,0
2,0
1,0
0
10^1
10^2
10^3
10^4
10^5
$r_w^2/\overline{\lambda_d^2}$
$k_a = 0$
$k_b = 0$
n = 0
TH "A"
TH "B"
TH "C" C
EXP
C
C

FIG. 13

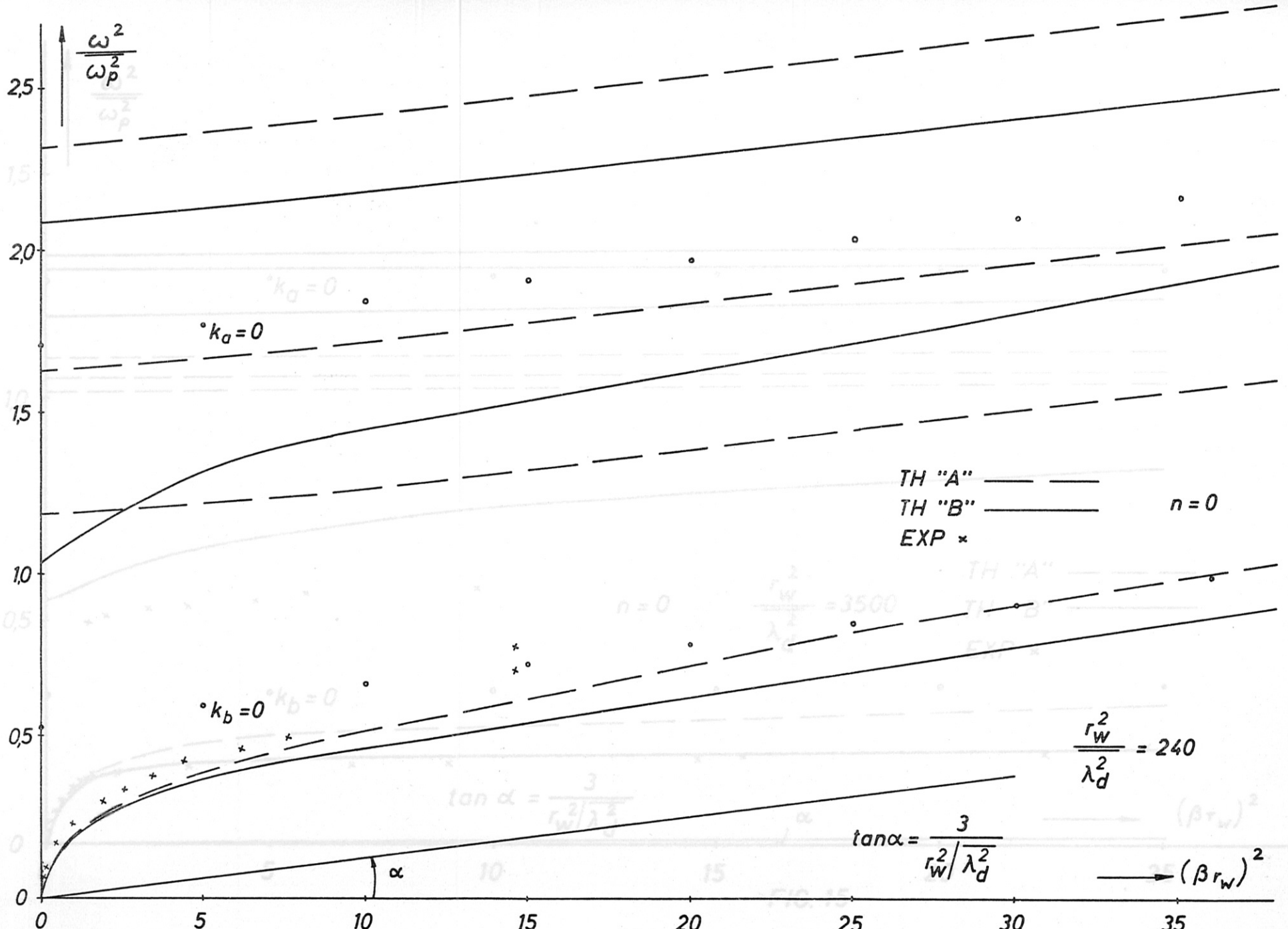
$\frac{\omega^2}{\omega_p^2}$
2,5
2,0
1,5
1,0
0,5
0
$^{\circ}k_a = 0$
$^{\circ}k_b = 0$
TH "A"
TH "B"
EXP ×
n = 0
$\frac{r_w^2}{\lambda_d^2} = 240$
$\tan\alpha = \frac{3}{r_w^2/\lambda_d^2}$
α
$(\beta r_w)^2$
0
5
10
15
20
25
30
35

FIG. 14

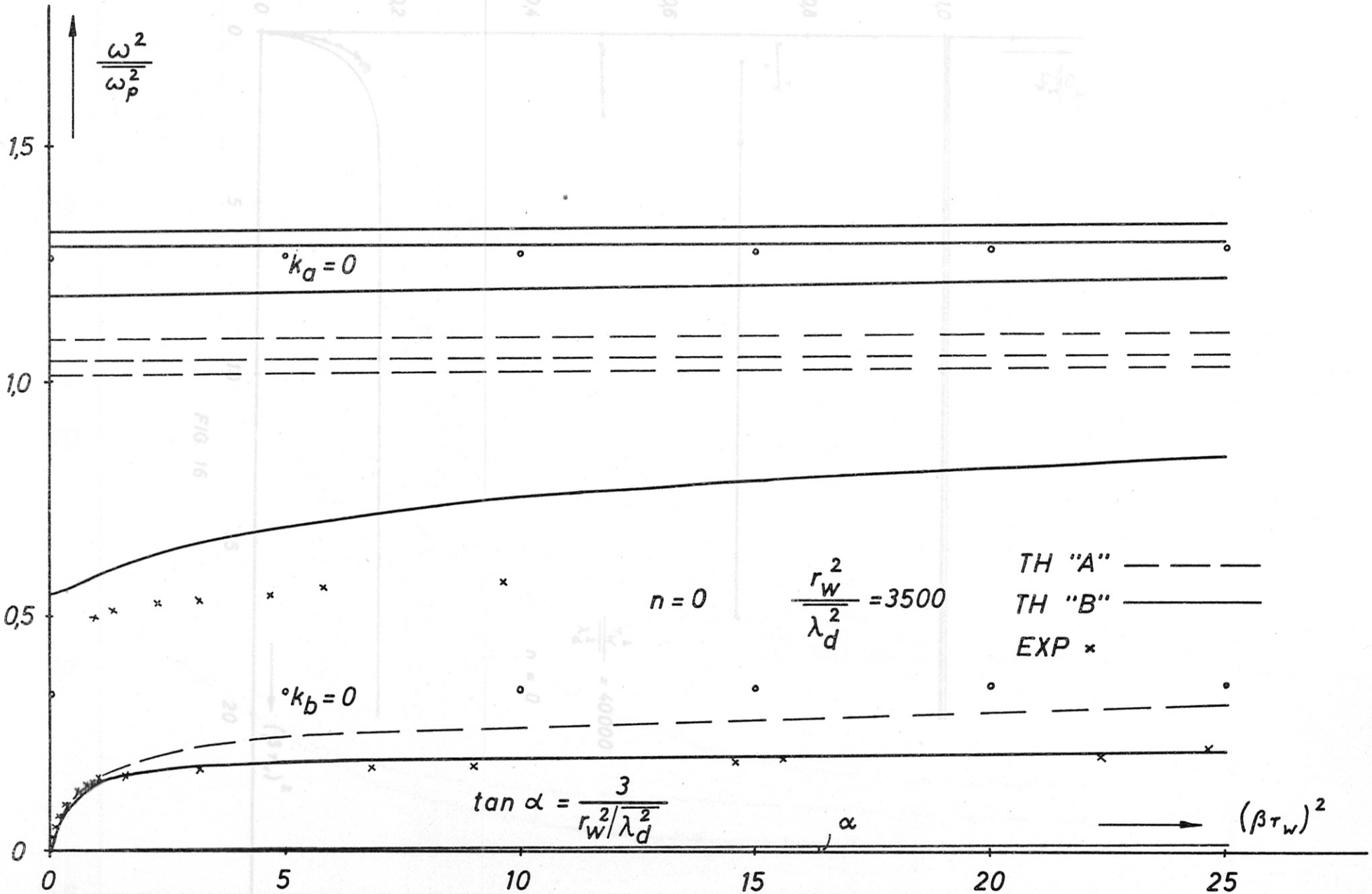
$\frac{\omega^2}{\omega_p^2}$
1,5
1,0
0,5
0
$^{\circ}k_a = 0$
$^{\circ}k_b = 0$
$n = 0$
$\frac{r_w^2}{\lambda_d^2} = 3500$
TH "A"
TH "B"
EXP ×
$\tan\alpha = \frac{3}{r_w^2/\lambda_d^2}$
α
$(\beta r_w)^2$
0
5
10
15
20
25

FIG. 15

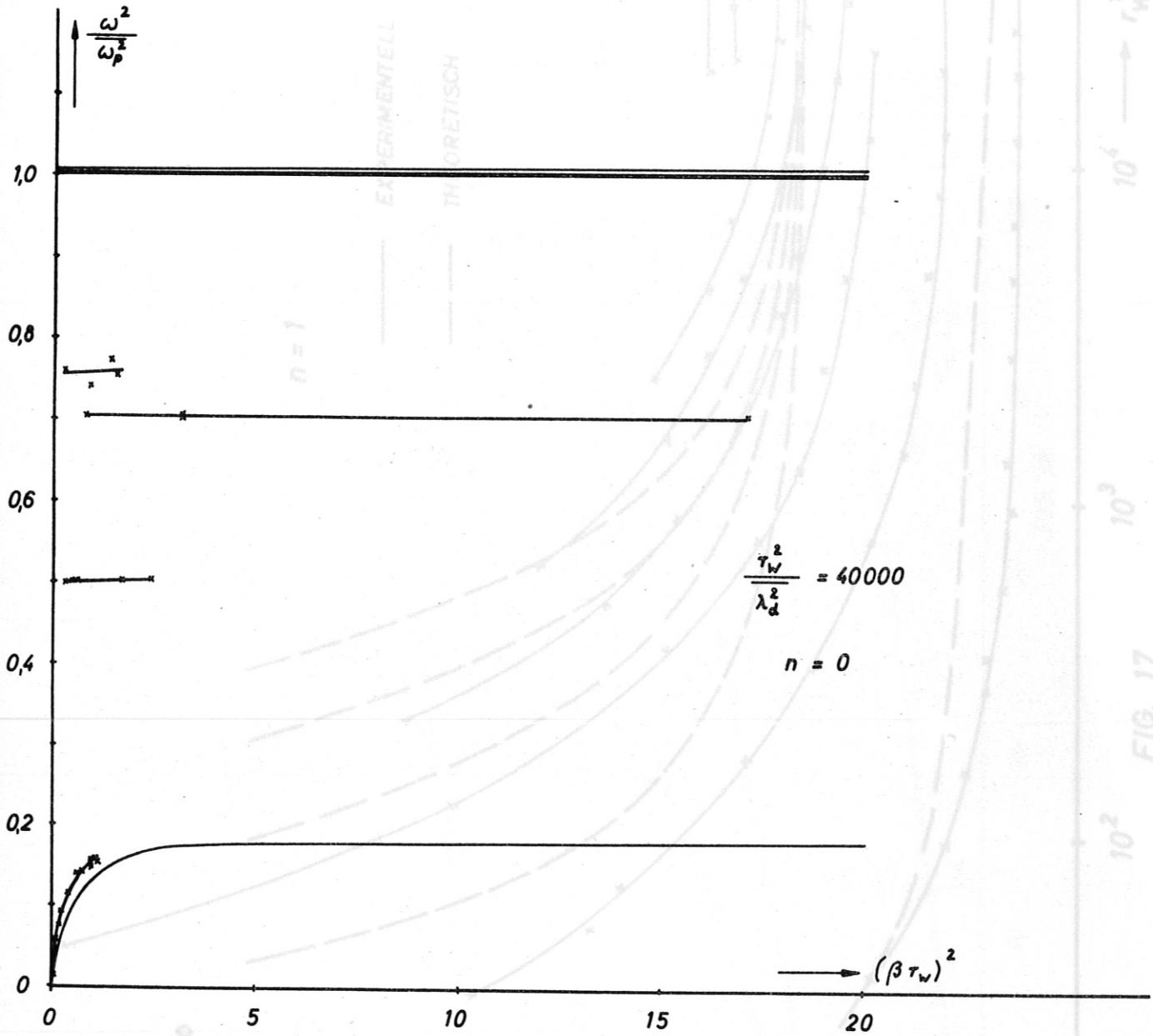
$\frac{\omega^2}{\omega_p^2}$
1,0
0,8
0,6
0,4
0,2
0
0
5
10
15
20
$(\beta r_w)^2$
$\frac{r_w^2}{\lambda_d^2} = 40000$
$n = 0$

FIG. 16

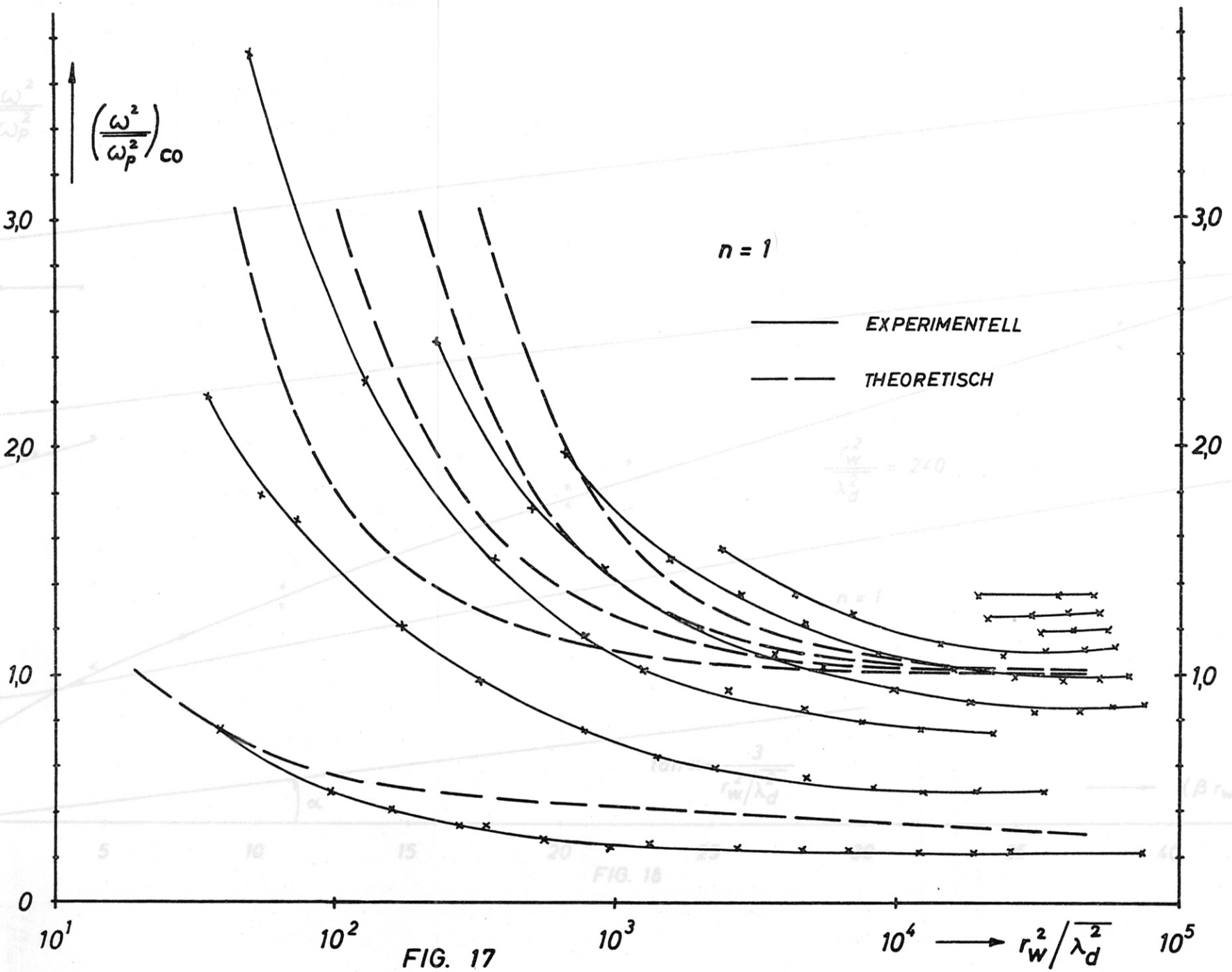
$\left(\frac{\omega^2}{\omega_p^2}\right)_{co}$
3,0
2,0
1,0
0
n = 1
EXPERIMENTELL
THEORETISCH
10^1
10^2
10^3
10^4
$r_w^2/\overline{\lambda_d^2}$
10^5

FIG. 17

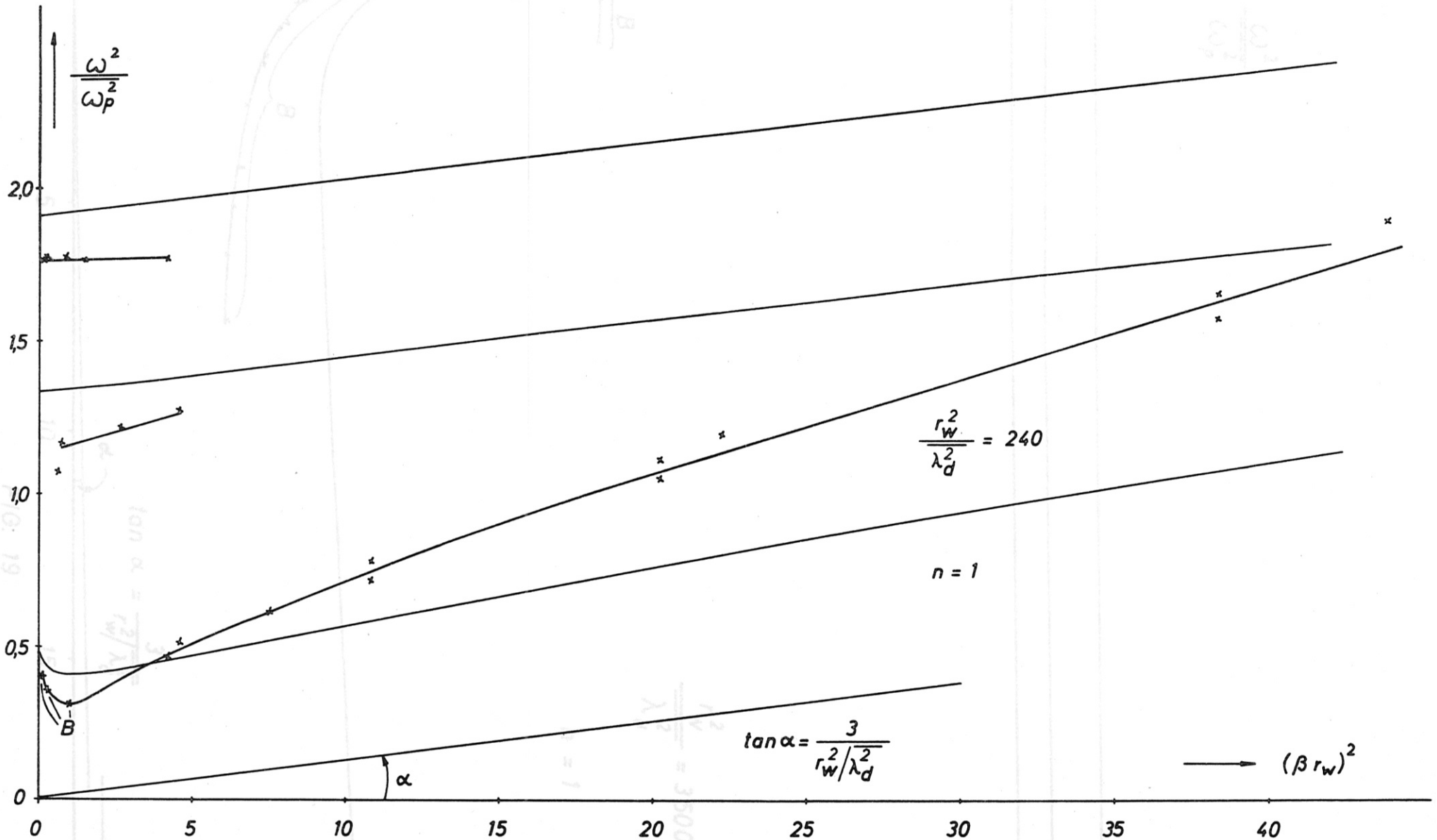
$\frac{\omega^2}{\omega_p^2}$
2,0
1,5
1,0
0,5
0
0
5
10
15
20
25
30
35
40
$\frac{r_w^2}{\lambda_d^2} = 240$
n = 1
B
$\tan\alpha = \frac{3}{r_w^2/\lambda_d^2}$
α
$(\beta r_w)^2$

FIG. 18

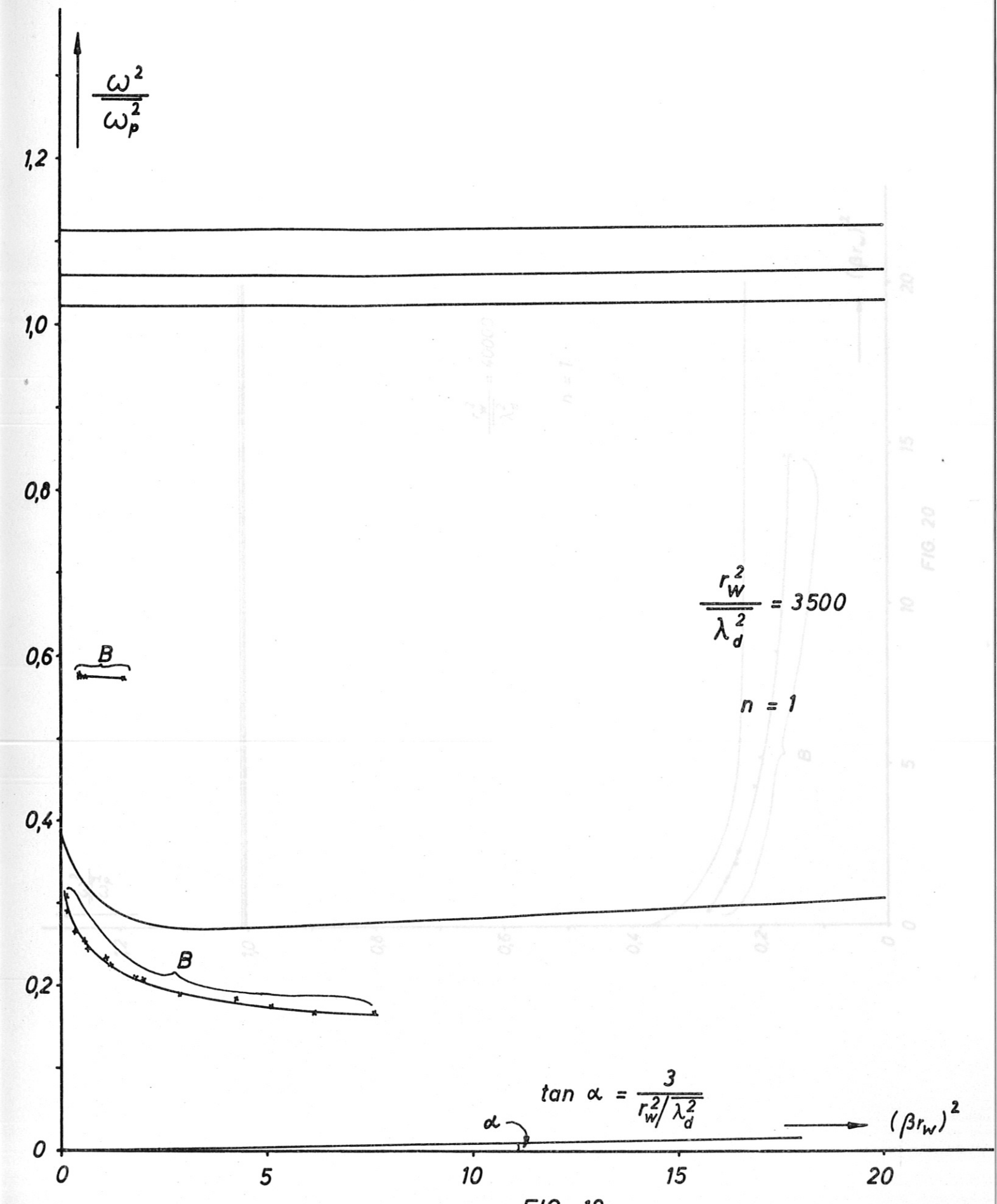
$\frac{\omega^2}{\omega_p^2}$
1,2
1,0
0,8
0,6
0,4
0,2
0
B
B
$\frac{r_w^2}{\lambda_d^2} = 3500$
$n = 1$
$\tan \alpha = \frac{3}{r_w^2/\lambda_d^2}$
α
$(\beta r_w)^2$
0
5
10
15
20

FIG. 19

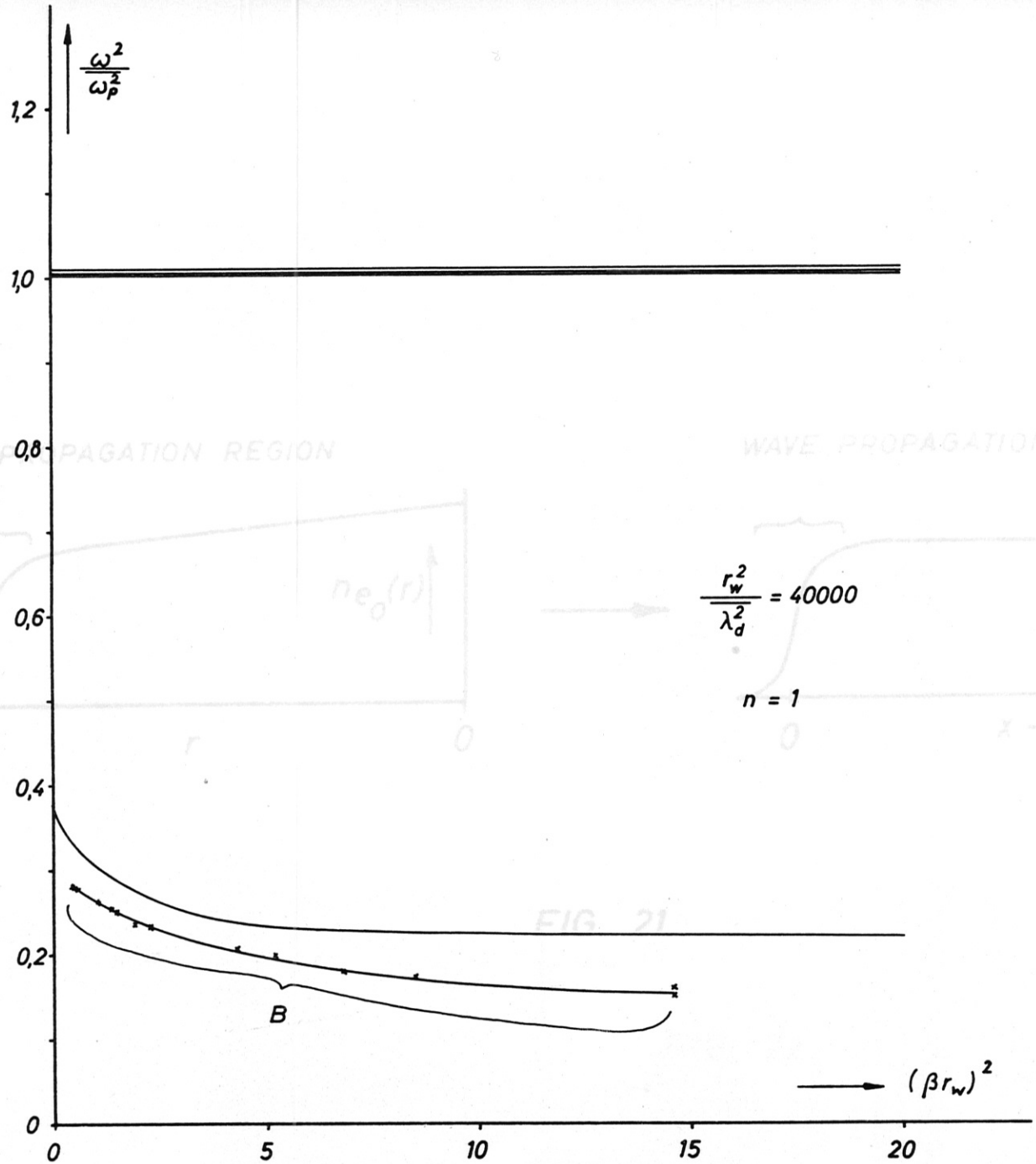
$\frac{\omega^2}{\omega_p^2}$
1,2
1,0
0,8
0,6
0,4
0,2
0
$\frac{r_w^2}{\lambda_d^2} = 40000$
n = 1
B
$(\beta r_w)^2$
0
5
10
15
20

FIG. 20

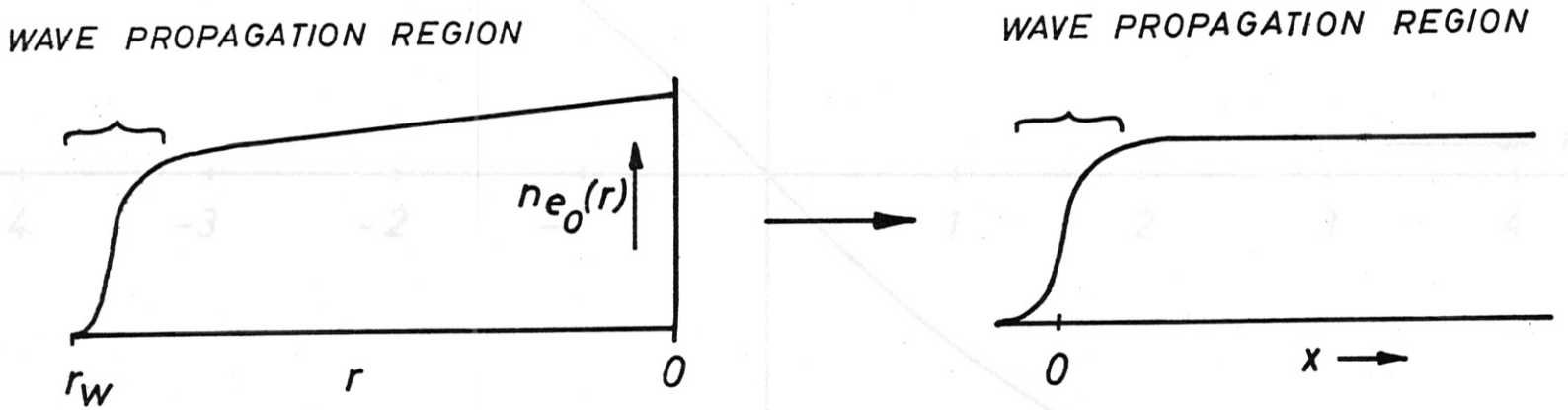
WAVE PROPAGATION REGION
$n_{e_0}(r)$
r_w
r
0
WAVE PROPAGATION REGION
0
x

FIG. 21

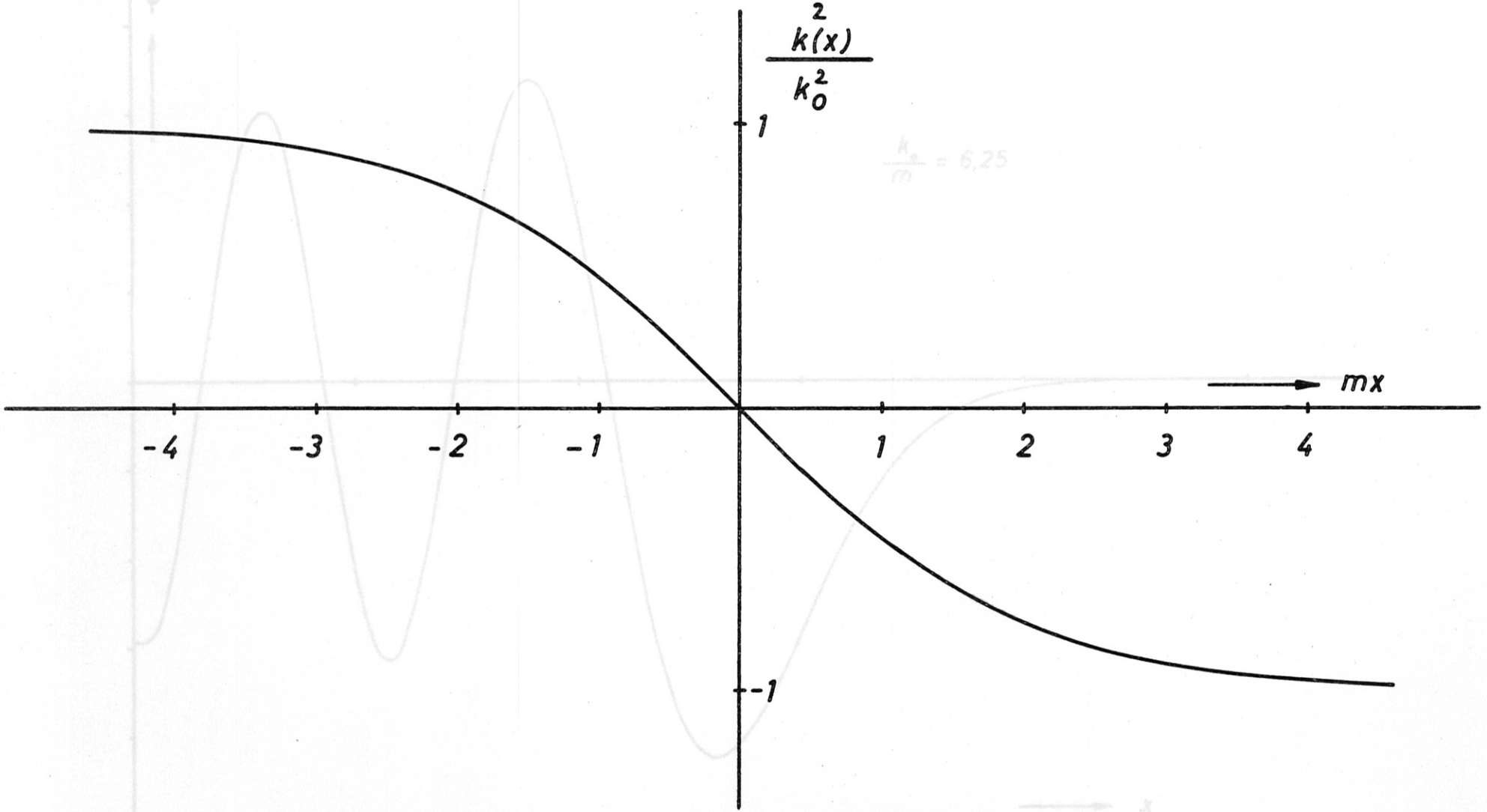

FIG. 22

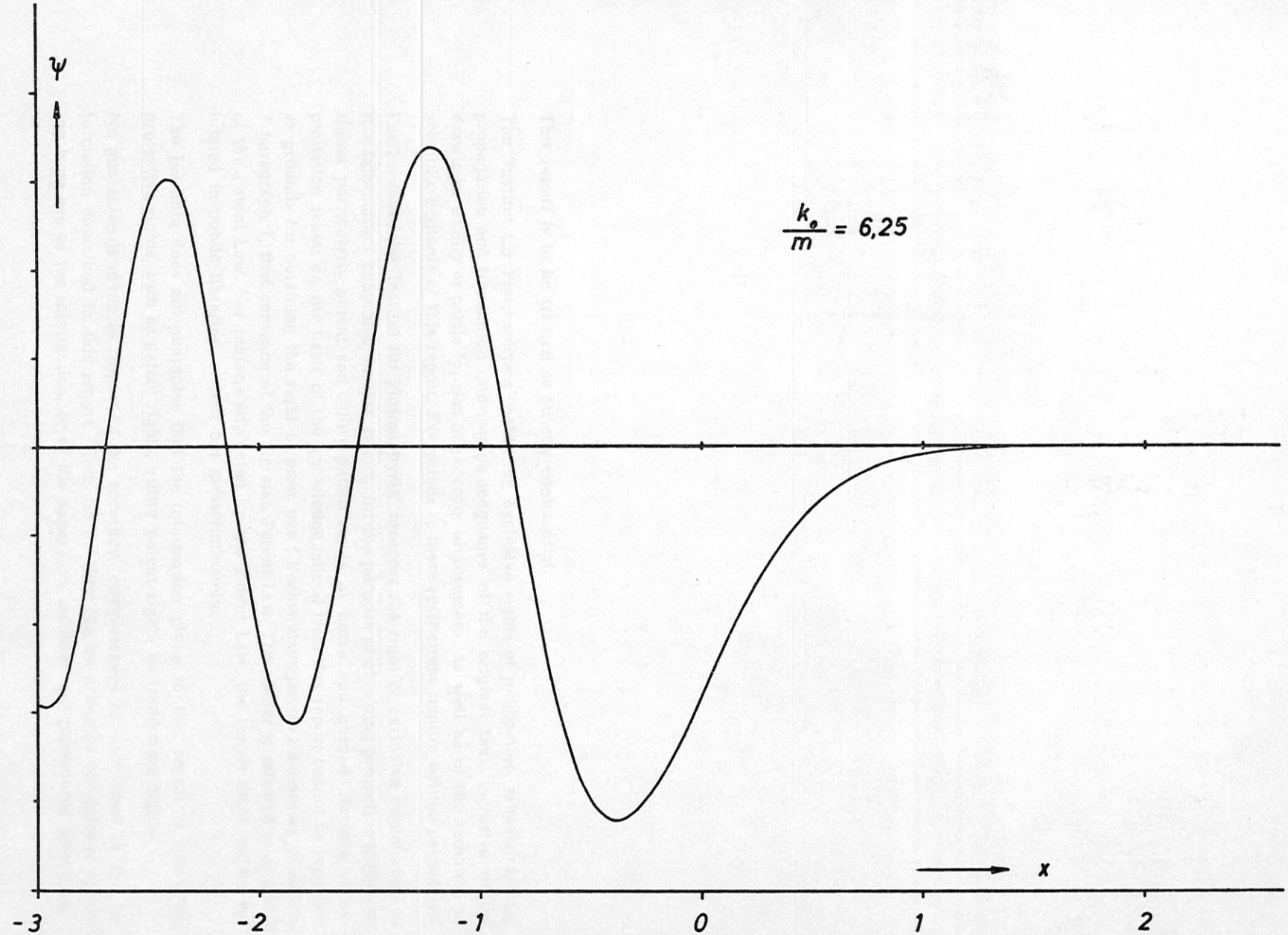

FIG. 23